



MOW strengthening and contourite development over two analog climate cycles (MIS 12–11 and MIS 2–1) in the Gulf of Cadíz: An impact on North Atlantic climate during deglaciation V and MIS 11?

Paul Moal-Darrigade^{a,*}, Emmanuelle Ducassou^a, Jacques Giraudeau^a, André Bahr^b, Stefanie Kaboth-Bahr^c, Vincent Hanquiez^a, Marie-Claire Perello^a

^a Université de Bordeaux, UMR CNRS 5805 EPOC, Allée Geoffroy St Hilaire, 33615 Pessac, France

^b Institute of Earth Sciences, Heidelberg University, Im Neuenheimer Feld 234, 69120 Heidelberg, Germany

^c Institute of Geosciences, University of Potsdam, Karl-Liebknecht-Straße 24-26, 14476 Potsdam-Golm, Germany

ARTICLE INFO

Editor: Fabienne Marret-Davies

Keywords:

Gulf of Cadíz
IODP sites U1386-U1387
Mediterranean outflow
MIS 12–11 vs. MIS 2–1
Contourites
Grain size

ABSTRACT

High-resolution records from International Ocean Discovery Program (IODP) sites U1386 and U1387 drilled during IODP Expedition 339 into the Faro drift, made it possible to assess the impact of intensifications of the upper core (MOW_U) of the Mediterranean Outflow Water (MOW) and of changes in sediment supply on the sedimentation in the northern Gulf of Cadíz since the Middle Pleistocene. This work focuses on the comparison of records covering Marine Isotope Stage (MIS) 2–1 and MIS 12–11, in order to investigate the behaviour and circulation regime of the MOW_U over two climatic cycles of similar astronomical configurations and their associated deglaciation. The analysis of facies established on the basis of grain size, XRF core-scanning, and carbonate content revealed contourite beds formed by the MOW_U during MIS 11 and MIS 1 and deglaciations (deglaciation V and I). Contourite sequences show that MOW_U velocity at the seabed was higher during MIS 2–1 than during MIS 12–11, and that sediment supply was different between these two climatic cycles. While overall low during MIS 12–11, MOW_U intensity increased during deglaciation V and MIS 11 and preceded large ice rafted events and cooling in the North Atlantic Ocean. As a major element of the MOW, MOW_U strengthening during deglaciation V likely contributed to higher heat and moisture transport towards the high latitudes inducing a slight increase of calving and size of boreal ice sheets. The MOW-derived injection of heat and salt in the North Atlantic Ocean during deglaciation V might have contributed, through reactivation of the upper AMOC, to the switch of the Atlantic thermohaline circulation from a glacial to an interglacial mode.

1. Introduction

Contourite drifts are defined as sediment bodies characterized by a major accumulation of sediment deposited or reworked by a bottom current (Heezen et al., 1966; Stow et al., 2002; Rebesco et al., 2008, 2014). The high sedimentation rates of these drifts make them precious archives for high resolution paleoceanographical studies (e.g., Brunner, 1986; Robinson and McCave, 1994; Harris et al., 2001).

Located off the southwestern sector of the Iberian margin, the Gulf of Cadíz is one of the most studied Contourite Depositional System (CDS) in the world ocean (e.g., Faugères et al., 1984; Hernández-Molina et al., 2006; Mulder et al., 2006; Hanquiez et al., 2007; Marchès et al., 2007; Llave et al., 2007; Brackenridge et al., 2013; Stow et al., 2013; Alonso

et al., 2016; Mestdagh et al., 2019). Its morphology is essentially shaped by the activity of the Mediterranean Outflow Water (MOW). Strongly influenced by the African monsoon system, MOW contributed to propagate (sub) tropical climate signals into the high latitudes during the Late Pleistocene (Bahr et al., 2015; Voelker et al., 2015a), impacting the Atlantic Meridional Overturning Circulation (AMOC) (Rogerson et al., 2006; Voelker et al., 2006; Bahr et al., 2015).

The Contourite Depositional System of the Gulf of Cadíz, has been extensively studied for high resolution reconstruction of MOW dynamics over the last 50 kyrs (Sierro et al., 1999; Rogerson et al., 2005; Llave et al., 2006; Voelker et al., 2006; Toucanne et al., 2007). Many studies support an enhancement of the lower branch of the MOW (MOW_L) during cold periods of the last glacial-interglacial cycle, synchronously

* Corresponding author.

E-mail address: paul.moal@u-bordeaux.fr (P. Moal-Darrigade).

<https://doi.org/10.1016/j.gloplacha.2021.103721>

Received 12 November 2020; Received in revised form 29 October 2021; Accepted 18 November 2021

Available online 11 December 2021

0921-8181/© 2021 Elsevier B.V. All rights reserved.

with abrupt climate changes in the North Atlantic (e.g., Sierro et al., 1999; Schönfeld and Zahn, 2000; Voelker et al., 2006). Some authors also observed a strong upper branch of the MOW (MOW_U) during cooling events in the Northern Hemisphere (Llave et al., 2006; Toucanne et al., 2007; Bahr et al., 2015; Sierro et al., 2020). However, it has been shown that MOW_U only shows strengthening during warm intervals (Llave et al., 2006; Kaboth et al., 2016; Sierro et al., 2020). Sedimentological analyses, suggest that the composition of sediments in the Gulf of Cadiz is only partly related to changes in bottom current velocity, as changes in sediment supply by rivers can also play an important role in sediment distribution (Mulder et al., 2013). The recent recovery of long sediment sequences from the Faro drift during IODP Expedition 339 (Hernández-Molina et al., 2014) offers a unique opportunity to extend the chronological framework of MOW reconstruction to older climatic cycles of the Middle Pleistocene, and to test the reliability of sedimentological parameters as proxies of current strength in the Gulf of Cadiz.

The present high resolution sedimentological and micropaleontological study is based on two Faro drift sediment records recovered at IODP sites U1386 and U1387, both covering, the Marine Isotope Stages (MIS) 2–1 (~ last 29 kyrs) and MIS 12–11 (~478–374 kyrs BP) intervals. These two sites are located 4 km apart and thus provide insights into the potential spatial variability of sedimentation in contourite drifts. MIS 2–1 and MIS 12–11 have been chosen for their similarities in Earth orbital configuration (Loutre and Berger, 2003). Despite differences in deglaciation patterns and slight discrepancies in orbital configuration (i. e. in the phasing of precession and obliquity) between MIS 11 and MIS 1 (e.g. Loutre and Berger, 2000; Rohling et al., 2010), their common weak eccentricity forcing and resulting similar insolation signals led to consider these two interglacials as close analogues (Loutre and Berger, 2000, 2003). This analogy also refers to comparable MIS 11 vs. pre-industrial MIS 1 greenhouse gas concentrations (CO₂ and CH₄), global atmospheric and ocean temperatures, global mean sea-level, and local sea-surface conditions (e.g., Petit et al., 1999; Droxler and Farrell, 2000; McManus et al., 2003; de Abreu et al., 2005; Raynaud et al., 2005; Siegenthaler et al., 2005; Spahni et al., 2005; Jouzel et al., 2007; Bowen, 2010). Hence MIS 11 has often been considered as the best analogue to the Holocene among the recent interglacials (e.g., Droxler and Farrell, 2000; Loutre and Berger, 2003; de Abreu et al., 2005; Palumbo et al., 2019). Some studies based on sediments of the Portuguese margin, close to our study area, evidence similar local sea-surface conditions and dynamics during these interglacials (de Abreu et al., 2005; Rodrigues et al., 2011; Palumbo et al., 2019). MIS 12, which is considered as one of the the most extreme glacial stage of the last 500 kyrs, shows very similar millennial time-scale variations than those characterizing the last glacial period -MIS 2- (McManus et al., 1999). Moreover, global atmospheric temperatures and Western Iberian sea-surface conditions were comparable during both glacials (e.g., Jouzel et al., 2007; Rodrigues et al., 2011; Palumbo et al., 2019).

The MIS 2–1 interval is the best studied glacial-interglacial cycle albeit MIS 1 does not represent an entire interglacial. Comparing the MIS 12–11 cycle to the MIS 2–1 interval serves as a test for previously established models of MOW dynamics (e.g. Llave et al., 2006). We make use of grain size characteristics and the geochemical composition of sediments to define distinct facies with the objective of understanding the impact of bottom current velocity and sediment supply changes on sedimentation patterns during these two comparable periods. Then, using our record of MOW_U activity during MIS 11, we evaluate the possible connection between MOW and the North Atlantic Climate during an analogue of the current interglacial (Loutre and Berger, 2000, 2003).

2. Regional setting

The present-day circulation in the Gulf of Cadiz is driven by exchanges through the Strait of Gibraltar where relatively low density (less saline) North Atlantic Water penetrates into the Mediterranean Sea at

surface, while denser Mediterranean Water flows into the Atlantic Ocean at depth (e.g., Bryden and Stommel, 1984; Bryden et al., 1994; Baringer and Price, 1999; Naranjo et al., 2015). The MOW which circulates northward following the continental slope (Ambar and Howe, 1979; Hernández-Molina et al., 2006, 2014; Mulder et al., 2006) is the principal water mass at intermediate depths in the Gulf of Cadiz. This saline Mediterranean water is located above the North Atlantic Deep Water (Baringer and Price, 1999; Hernández-Molina et al., 2014) and is overlaid by the sub-polar variety of North Atlantic Central Water (Voelker et al., 2015b).

The MOW, which flows at a rate of about 1.78 Sv through the Strait of Gibraltar (Bryden and Stommel, 1984; Bryden et al., 1994), is principally composed of Levantine Intermediate Water (LIW) produced in the Eastern Mediterranean Sea (Millot et al., 2006; Millot, 2009, 2014) and of variable proportions of Western Mediterranean Deep Water formed in the Gulf of Lion and in the Alboran and Tyrrhenian Seas (Millot, 2014). LIW is the dominant water mass composing MOW, inferring that deep and intermediate water formation in the Eastern Mediterranean Sea is a key driver of MOW production (Rogerson et al., 2012; Toucanne et al., 2012; Millot, 2014).

Upon leaving the Strait of Gibraltar and entering the Gulf of Cadiz, MOW splits into two main flows under the influence of the complex morphology of the continental slope: the Mediterranean Upper Water (MOW_U) and the Mediterranean Lower Water (MOW_L). MOW_L flows between 800 and 1400 m depth alongside the middle slope, and is subdivided into three minor branches due to slope morphology (e.g. Madelain, 1970; Ambar and Howe, 1979; Borenäs et al., 2002). Following the base of the upper slope at depths of 400–700 m (Ambar, 1983; Ambar et al., 2002; Hernández-Molina et al., 2011, 2014), the MOW_U flows northward into the Gulf of Cadiz. MOW velocity gradually decreases northward from 300 cm.s⁻¹ in the Strait of Gibraltar to 10–30 cm.s⁻¹ at the latitude of Cape Saint Vincent (Ambar and Howe, 1979). Bottom current velocity is however highly variable locally due to sea-floor irregularities (Hernández-Molina et al., 2006; García et al., 2009; Stow et al., 2009; Serra et al., 2010)

The Contourite Depositional System of the Gulf of Cadiz results from the complex interaction between bottom water currents of the MOW and the middle slope of the southwest Iberian margin (Madelain, 1970; Faugères et al., 1984; Nelson and Maldonado, 1999; Stow et al., 2002; Mulder et al., 2006; Hernández-Molina et al., 2006; Hanquiez et al., 2007; Marchès et al., 2007). The generated drift deposits, such as the Faro drift studied in this paper, are composed of different proportions of muddy, silty and sandy sediment of mixed terrigenous and biogenic composition (e.g., Gonthier et al., 1984; Stow et al., 1986).

A series of papers based on the study of CDS sediments demonstrate the relation between the behaviour of the MOW and different climatic events during the late Quaternary (e.g. Nelson and Maldonado, 1999; Schönfeld and Zahn, 2000; Rogerson et al., 2005; Llave et al., 2006; Voelker et al., 2006; Toucanne et al., 2007; Bahr et al., 2014, 2015; Kaboth et al., 2017). It appears that during the Pleistocene, the African monsoon had a strong influence on MOW variability on orbital-scales (Bahr et al., 2015; Voelker et al., 2015a; Sierro et al., 2020). At glacial-interglacial time scales, the multiple branches of the MOW occupy a different spatial position and fluctuate in their flow strength during warm vs. cold climatic periods due to varying densities of the outflowing water masses (Schönfeld and Zahn, 2000; Rogerson et al., 2005; Hernández-Molina et al., 2006; Llave et al., 2006; Voelker et al., 2006; Rogerson et al., 2012). Sediments in the Gulf of Cadiz have recorded further modifications of the character of the MOW linked to the influence of North Atlantic climate oscillations, with a strengthened MOW during Heinrich Stadials (HS) and Dansgaard-Oeschger (DO) stadials (Llave et al., 2006; Voelker et al., 2006; Toucanne et al., 2007). These findings are supported by models which show increased convection in the North Atlantic when the MOW is the strongest (Bigg and Wadley, 2001), even if the exact impact of the MOW on AMOC remains unclear (Swingedouw et al., 2019).

3. Material & methods

3.1. IODP Sites U1386 and U1387

This study is based on two sites drilled during IODP Expedition 339 (Stow et al., 2013) from November to January 2011/2012. IODP sites U1386 and U1387 lie off the southern Iberian margin, at 36°49.685'N, 7°45.321'W and 561 m depth, and 36°48.321'N, 7°43.1321'W and 560 m water depth, respectively (Fig. 1). Both IODP sites are presently bathed by the upper branch of the MOW but Site U1386 is positioned closer to the moat generated by the MOW_U (Hernández-Molina et al., 2013). Sediment samples were selected following the shipboard splice of IODP Sites U1386 and U1387 which joins core sections from Holes A and B (Expedition 339 Scientists, 2012). The high-resolution XRF scanning and grain size analyses of the sediment from the deepest interval of IODP Site U1386 suggests that the shipboard splice in this depth interval based on physical property correlations (Stow et al., 2013) required modifications. In more detail, we find that the previous core-to-core transition (A15-B14) divided a contourite layer in the middle, that we corrected according to XRF scanning records and grain size measurements (Fig. 2). The corrected meters composite depth (c-mcd) scale used in this paper presents a correction of +0.17 m between the core U1386A-15H and U1386B-14H. This paper focuses on the intervals which correspond to 0–10 m composite depth (mcd) and 126–162 (c-mcd) for IODP Site U1386 and 0–9 mcd and 95–125 mcd for IODP Site U1387.

3.2. Radiometric analyses of IODP Site U1386

Seven radiocarbon measurements were performed on mix, visually clean, handpicked planktic foraminiferal tests from the >150 μm fraction, according to Ducassou et al. (2018). Ages were determined at the Laboratoire de Mesure du Carbone 14 Saclay (Paris). The calibration of radiocarbon age to calendar years was performed using the Calib Rev. 7.0.2 program/ Marine20 data set (Reimer et al., 2009). Here, we chose to present the median probability of the ages (Telford et al., 2004).

3.3. Foraminiferal analyses

The biostratigraphy of IODP Site U1386 was performed at a

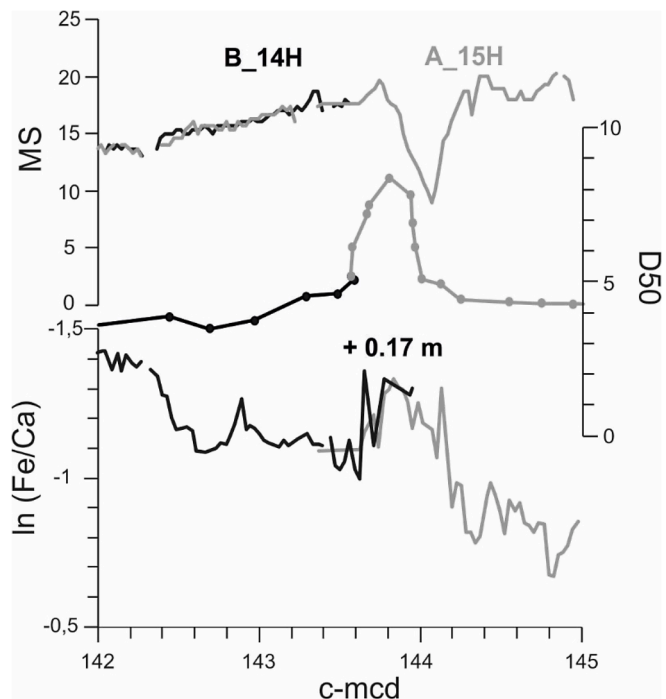


Fig. 2. Correction of the shipboard meter composite depth (mcd) scale of core B_14H (black) and core A_15H (grey) using several parameters including a) magnetic susceptibility (MS), b) median grain size (D₅₀), and c) XRF derived Fe/Ca ratio. + 0.17 m corresponds to the length of sediment column added to the splice.

resolution close to 25 cm for both intervals. The resolution of faunal analyses for IODP Site U1387 was higher (20 cm) in the upper interval than in the lower one (41 cm). The samples were washed and sieved in order to extract the >63 μm fraction. The residues were dried and weighed and the >150 μm fraction was separated for foraminiferal counts.

Planktic foraminiferal identification was performed in aliquots of the

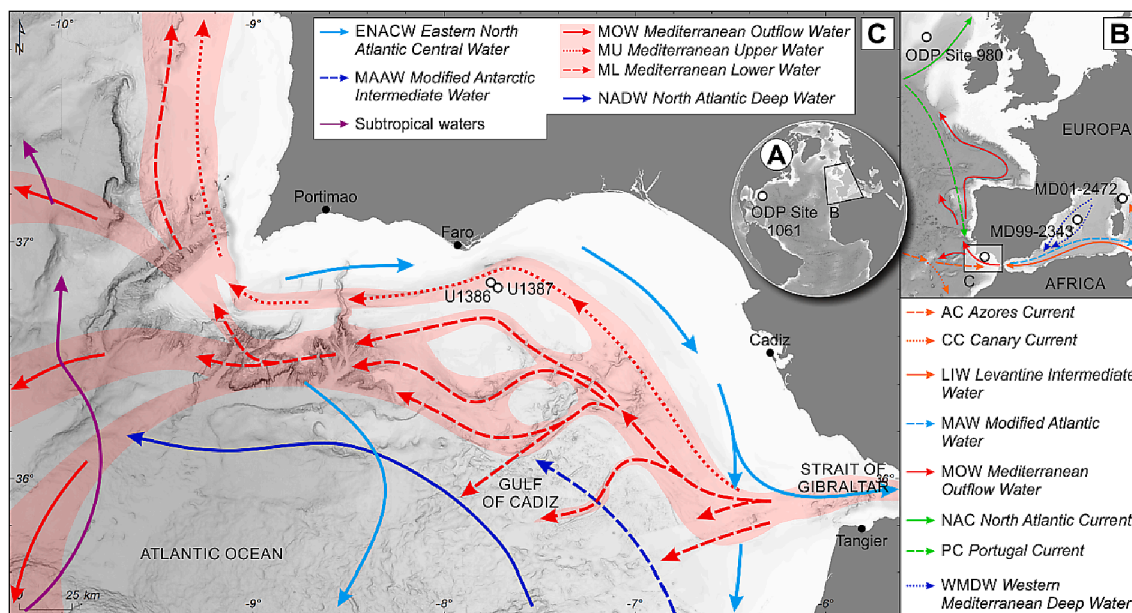


Fig. 1. A) Position of ODP Site 1061. B) General currents and water masses influencing the Gulf of Cadiz and location of deep-sea cores MD99-2343 and MD01-2472. C) IODP Sites U1386 and U1387 locations and major water masses of the Gulf of Cadiz (Demirov and Pinardi, 2007; Carracedo et al., 2016; Hernández-Molina et al., 2016; Schroeder et al., 2017).

>150 μm fraction with total numbers of specimens exceeding 250, and according to Spezzaferri et al. (2015) and Schiebel and Hemleben (2017). In this study, special attention was directed towards the species *Negloboquadrina pachyderma*, *Globorotalia truncatulinoides*, *Globigerinoides ruber rosea*, *Globigerinoides conglobatus*, *Globorotalia crassaformis* and *Trilobatus sacculifer*. Species abundances were expressed in weight % according to total counts.

The abundance of the polar species *N. pachyderma* was used for tracing the presence of subpolar to polar surface waters in the south-western Iberian margins during cold events of Heinrich Stadials (e.g., Eynaud et al., 2009; Voelker et al., 2009; Ducassou et al., 2018).

G. ruber rosea, *G. conglobatus*, *G. crassaformis* and *T. sacculifer* are tropical and sub-tropical species and their abundance in sediments of the Gulf of Cadiz increased during the recent warm periods of the Holocene and the Bølling-Allerød (e.g., Sierro et al., 1999; Ducassou et al., 2018).

G. truncatulinoides is a subtropical deep dwelling species and is a good indicator of the thermocline location (e.g., Be, 1960). Coiling directions of *G. truncatulinoides* are given as percentages of the sinistral coiling ratio, using the formula: $\text{GTS} = \text{GTS} * 100 / (\text{GTS} + \text{GTD})$, where GTS is the number of specimens of *G. truncatulinoides* sinistral and GTD the number of specimens of *G. truncatulinoides* dextral (Ducassou et al., 2018). This coiling ratio was calculated only when the number of specimens represented at least 0.5% of the total assemblage.

3.4. X-ray fluorescence analysis

High-resolution X-ray fluorescence (XRF) scanning was conducted along the split core of U1386, from 125 to 165 mcd, using an Avaatech XRF corescanner III at Center for Marine Environmental Sciences (MARUM, University of Bremen). The XRF III scanner is equipped with an Oxford Instrument 100 W Neptune X-ray tube with Rhodium (Rh) target. Measurements were conducted every 3 cm over a 1.2 cm^2 area with a down-core slit size of 12 mm and a sampling time of 20 s. Two separate runs were performed using generator settings of 10 kV and 0.4 mA, and 30 kV and 1.0 mA. The split core surface was covered with a 4 μm -thin SPEXcerti Prep Ultralene foil to avoid sediment desiccation and contamination between XRF measurements. The data were acquired by a Canberra W-PIPS Silicon Drift Detector (SDD; Model SXD 15C-150–500) with 150 eV X-ray resolution and the Canberra Digital Spectrum Analyzer DAS 1000. Raw data were processed by the analysis of X-Ray spectra by the Iterative Least square software (WIN AXIL) package from Canberra Eurisys. The 0–10 mcd interval of IODP Site U1386 was investigated with an AVAATECH XRF Scanner of the Royal Netherlands Institute for the Sea Research (NIOZ) (details given in Kaboth et al. (2016)). XRF measurements of U1387 material were performed at the MARUM-University of Bremen using an Avaatech XRF corescanner II (detail given in Bahr et al. (2014)). XRF core-scanning is a time efficient method for semi-quantitative elemental analysis of sediment. Individual elemental intensities (expressed in counts) can be influenced by changing lithology and by the formation of a water film below the covering foil (Tjallingii et al., 2007). These biases can be corrected by using elemental ratios (Bahr et al., 2014).

In the current study, we are presenting the $\ln(\text{Zr}/\text{Al})$ and $\ln(\text{Fe}/\text{Ca})$ records. The $\ln(\text{Zr}/\text{Al})$ ratio is a useful semi-quantitative indicator of bottom current velocity variations (Bahr et al., 2014). Furthermore, $\ln(\text{Fe}/\text{Ca})$ reflects the contribution of biogenic carbonate-rich particles versus detrital components in sediment supply.

3.5. Sedimentological analyses

Grain size analyses were performed on the bulk sediment, at 5 cm intervals in coarser sequences and at 100 cm (U1386) and 150 cm (U1387) resolutions in homogeneous muddy sequences, using a Malvern MASTERSIZER S (University of Bordeaux, UMR 5805 EPOC). In the topmost interval of IODP Site U1386 (0–10 mcd), grain size analyses were also performed on decarbonated samples. Measurements of

median grain size (D_{50}), percentage of sand and sortable silt mean size (SS; McCave et al. (1995)) were used here as indexes of bottom flow speed according to McCave and Hall (2006). To make up for the lack of decarbonated grain size measurements on the deepest intervals carbonate content was measured using a Bernard calcimeter between 129 and 162 c-mcd of IODP Site U1386. We collected 12 samples of 50–130 mg on the deepest interval of IODP Site U1386, at different strategic locations chosen according to the $\ln(\text{Fe}/\text{Ca})$ ratio. In the >150 μm fraction, lithic grain, including quartz grains, were counted and expressed as number per gram of dry weight of bulk sediment.

4. Chronostratigraphy of IODP Sites U1386 and U1387

4.1. Stratigraphy of IODP Site U1386

The initial chronology for both MIS 12–11 and MIS 2–1 intervals at IODP Site U1386 is based on the visual alignment of the benthic stable oxygen isotope record from IODP Site U1386 to the global benthic $\delta^{18}\text{O}$ record of LR04 (Kaboth et al., 2017). For the interval MIS 2–1, the initial chronology was refined by six new AMS ^{14}C dates (Table 1), validating previous age models proposed by Bahr et al. (2015) and Kaboth et al. (2017) for the last 20 kyrs BP and slightly improving the chronology between 30 and 20 kyrs BP (Fig. 3). Based on the biostratigraphic framework and benthic $\delta^{18}\text{O}$ record, one of the seven AMS ^{14}C dates was not considered in the construction of the age model (Table 1 and Fig. 3).

The resulting sedimentation rates at the beginning of MIS 2 are very high at IODP Site U1386 (173 cm kyr^{-1}). The remaining interval of MIS 2 as well as the following deglaciation is characterized by a drop of sedimentation rate to 24.5 cm kyr^{-1} (Table 2). During the lower Holocene, rates briefly increase (up to 45 cm kyr^{-1}) before declining progressively to reach 16 cm kyr^{-1} during the upper Holocene (Table 2). This comparatively low sedimentation rate possibly reflects a low supply of sediment during the end of Holocene. According to sampling intervals, these various sedimentation rates result in a mean resolution of 0.46 kyrs between each planktic foraminiferal sample used to infer bioevents of IODP Site U1386.

We also slightly adapted the chronology for the MIS 12–11 time interval by modifying the applied mcd depth scale. During the MIS 12–11 cycle, mean sedimentation rates averaged 34 cm.kyrs^{-1} (Table 2) and the sampling interval allows for a mean time resolution of ~ 0.9 kyrs between each planktic foraminiferal sample.

4.2. Site-to-site correlation (U1386-U1387)

4.2.1. Planktic foraminifer distribution: A correlation tool

A sediment transport and sorting independent proxy based on planktic foraminifer distribution was used as a tuning target for the site-to-site correlation. Hence differences in MOW flow at both sites can be more independently assessed than by using other tuning such as Zr/Al signals. Transferring the age model from our reference IODP Site U1386 into U1387 (Fig. 4 and Table 3), is based on the following arguments. First, a recent study of Ducassou et al. (2018) showed that during the Late Pleistocene, bioevents based on planktic foraminifera from Gulf of Cadiz present similar ages regardless of sedimentary environments (contourite vs. hemipelagite). Second, some of the species are clearly related to rapid changes in surface water conditions in the Gulf of Cadiz which provide additional informations on the sedimentation conditions.

4.2.2. From planktic foraminifer assemblages to bioevent identification

By combining this chronology with the planktic foraminiferal assemblages, we identified four and six bioevents during the MIS 2–1 and MIS 12–11 periods, respectively. In order to facilitate the description of bioevents and the following discussion, and based on the recent nomenclature recommendation (Railsback et al., 2015), we divide MIS 12 and MIS 11 into three substages (12c, 12b 12a and 11c, 11b and 11a). The MIS 11c interval, which extends from 425 kyrs cal. BP to 398 kyrs

Table 1
New radiocarbon ages of IODP Site U1386 (this study). Bulk: mix of planktic foraminifera.

| Site | Depth (mcd) | Lab code | Species | Conventional AMS ¹⁴ C age (¹⁴ C yr BP) | Standard error | 95.4% (2 σ) cal yr BP age ranges | Cal yr BP age median probability | Remarks |
|-------|-------------|-------------|---------|---|----------------|----------------------------------|----------------------------------|---|
| U1386 | 0.18 | SacA 35,774 | Bulk | 2155 | ±30 | 1410–1707 | 1568 | |
| | 1.08 | SacA 35,775 | Bulk | 6735 | ±40 | 6870–7223 | 7044 | |
| | 1.68 | SacA 35,778 | Bulk | 8570 | ±40 | 8809–9217 | 9015 | |
| | 2.38 | SacA 35,779 | Bulk | 9805 | ±50 | 10,350–10,801 | 10,587 | |
| | 4.438 | SacA 35,776 | Bulk | 20,170 | ±100 | 23,012–23,674 | 23,325 | Assumed to be too old based on benthic δ ¹⁸ O and biostratigraphic framework |
| | 6.438 | SacA 35,777 | Bulk | 23,060 | ±140 | 26,027–26,864 | 26,433 | |
| | 13.61 | SacA 35,780 | Bulk | 27,230 | ±180 | 30,156–30,943 | 30,569 | |

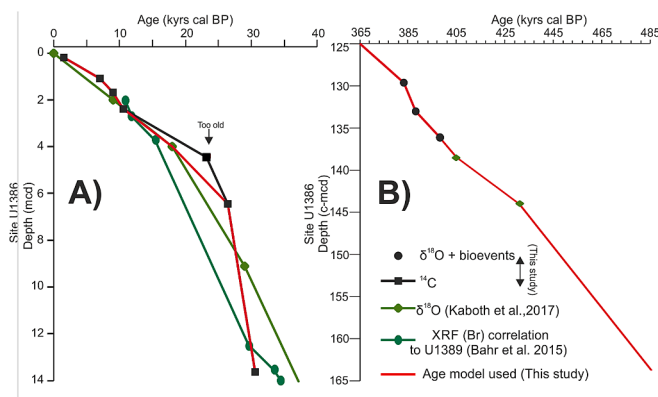


Fig. 3. A) Age model of IODP Site U1386 over the past 40 kyrs cal. B) Age model of IODP Site U1386 between 485 kyrs BP and 365 kyrs BP. Black circles indicate correlation points to northern Atlantic records (see Supplementary Data Fig. 1), black squares represent ¹⁴C-based control points, correlation points to LR04 are marked by light green diamond (Kaboth et al., 2017); dark green circles show correlation points (XRF-Br) to U1389. Tie points of IODP Site U1386 used for this study are indicated in Table 2. (For interpretation of the references to colour in this figure legend, the reader is referred to the web version of this article.)

cal. BP, corresponds to the interglacial period of the MIS 11 (Tzedakis et al., 2012b).

4.2.2.1. Holocene and MIS 11 foraminiferal assemblages. *G. ruber rosea*, *G. conglobatus*, *G. crassaformis* sinistral (s) and *T. sacculifer* were typically present during interglacial periods with abundance ranges of 0–5%, 0–3%, 0–2% and 1–10%, respectively. Our results show an increase of these warm species during the Holocene (Fig. 5) as previously described in the study area (Ducassou et al., 2018).

MIS 11 was overall characterized by high contributions (4–16%) of *T. sacculifer* with peak values reached during substage MIS 11c. The relative abundances of the accessory warm water species *G. ruber rosea* and *G. conglobatus* show maximum values (1–2%) during this substage. Rare occurrences (0.3–1.5%) of *G. crassaformis* (s) during MIS 11c and MIS 11a at both IODP sites U1386 and U1387 (Fig. 6) are used to improve the correlation between both sites when tuning based on the abundance of *G. truncatulinoides* (see below, section « 4.2.2.3. Coiling direction of *Globorotalia truncatulinoides*») is questionable.

4.2.2.2. Glacial and cold assemblages: YD, MIS 2 and MIS 12. Over the last 30 kyrs, at least three intervals of increased occurrences of the polar species *N. pachyderma* were observed, and were used to correlate IODP

Table 2
Tie points of IODP Site U1386 are based on ¹⁴C dates, alignment of isotopic events of δ¹⁸O benthic record at IODP Site U1386 (during MIS 11b) with δ¹⁸O benthic record from North Atlantic (see Supplementary data Fig. 1) and on a correlation between the δ¹⁸O benthic record (Kaboth et al., 2017) of IODP Site U1386 and the LR04 benthic stack of Lisiecki and Raymo (2005). ^aTie point used to correlate IODP Site U1386 record to LR04 benthic stack of Lisiecki and Raymo (2005) Kaboth et al., 2017). In black: correlation points of this study. In grey: tie point ruled out for this study.

| IODP Site U1386 depth (mcd and c-mcd) | Tie point age (Kyrns) | Sed. Rate (cm kyr ⁻¹) |
|---------------------------------------|-----------------------|-----------------------------------|
| 0.18 | 1.568 | |
| 1.08 | 7.044 | 16 |
| 1.68 | 9.015 | 30 |
| 2.38 | 10.587 | 45 |
| 4 ^a | 18 | 22 |
| 6.438 | 26.433 | 29 |
| 13.613 | 30.569 | 173 |
| 117.4 ^a | 341 | |
| 129.6 | 383 | 29 |
| 133 | 388 | 68 |
| 136.1 | 398 | 31 |
| 136 ^a | 401 | |
| 138.5 ^a | 405 | 34 |
| 144.17 ^a | 431 | 27 |
| 172.17 ^a | 508 | 33 |

Site U1387 to IODP Site U1386. The youngest interval, with mean values of 3%, encompasses the Younger Dryas (e.g., Rogerson et al., 2005; Voelker et al., 2006; Ducassou et al., 2018). In the Gulf of Cadiz, this bioevent was dated between 11,070 and 13,800 cal yr BP (Ducassou et al., 2018). The previous interval of peak occurrence of *N. pachyderma* (11–12%; Fig. 5) is linked to Heinrich Stadial 1 (18 to 15.6 cal kyr BP; Sanchez Goñi and Harrison (2010)) as identified by several authors (e.g., Turon et al., 2003; Ducassou et al., 2018). In the study area, this bioevent extends from 17,950 to 15,400 cal yr BP (Ducassou et al., 2018). The third period of high occurrence of *N. pachyderma* (ca. 3%) is older than 28,400 yr BP. Because of the different characteristics of this third bioevent compared to the two more recent ones, we propose that this final bioevent is related to Heinrich Stadial 3, as previously observed in other studies (e.g., Llave et al., 2006; Ducassou et al., 2018). Alike Voelker et al. (2009) who used *N. pachyderma* abundances in a core of the Gulf of Cadiz (MD99-2399) to reconstruct the hydrography of Iberian margins, we did not find any evidence of Heinrich Stadial 2 in planktic foraminiferal records of IODP sites U1386 and U1387. Abundance of *N. pachyderma* at sites U1386 and U1387 varied between 0 and 16% during MIS 12–11. Peak values of 8 and 16%, respectively, occurred during deglaciation V (Fig. 6) and were used to correlate IODP sites U1387 and U1386. Another correlating bioevent was identified

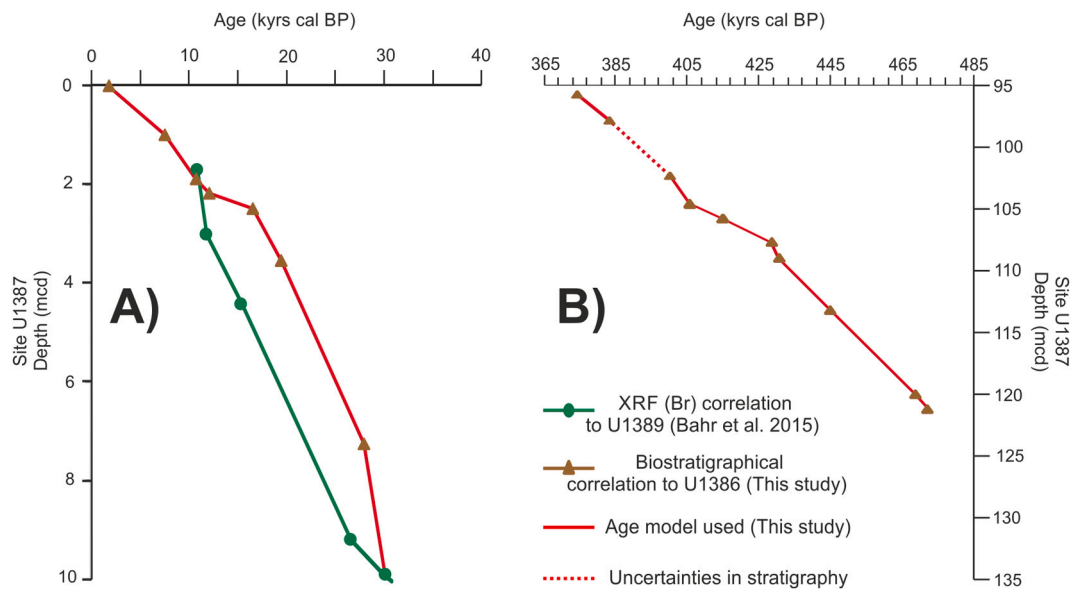


Fig. 4. A) Age model of IODP Site U1387 over the past 40 kyr cal BP. B) Age model of IODP Site U1387 between 485 kyr BP and 365 kyr BP; dark green circles show correlation points (XRF-Br) to U1389 (Bahr et al., 2015); brown triangles represent planktic foraminiferal correlation points between sites U1387 and U1386 and red line represents age models used in this study. Tie points in IODP Site U1387 are given in Table 3. (For interpretation of the references to colour in this figure legend, the reader is referred to the web version of this article.)

Table 3

Stratigraphic tie points in IODP Site U1387 based on correlations of planktic foraminiferal abundances (*N. pachyderma*, *G. truncatulinoides* and *G. crassaformis* (s) with bioevents identified in IODP Site U1386, and XRF-Br correlations to U1389 (Bahr et al., 2015). ^b Tie point used to correlate the XRF-Br of IODP Site U1386 to IODP Site U1389 (Bahr et al., 2015). Sedimentation rate in *italics* has to be considered carefully because of uncertainty about the age model.

| IODP Site U1387 depth (mcd) | Tie point ages (kyrs) | Sedimentation rate (cm. kyr ⁻¹) |
|-----------------------------|-----------------------|---|
| 0 | 1.568 | |
| 1.01 | 7.442 | 17 |
| 1.9 | 10.656 | 28 |
| 2.19 | 12 | 22 |
| 2.5 | 16.49 | 7 |
| 3.55 | 19.4 | 36 |
| 7.25 | 27.9 | 44 |
| 9.91 ^b | 30.09 | 121 |
| 95.7 | 374 | |
| 97.8 | 383 | 23 |
| 102.3 | 400 | 26 |
| 104.6 | 405.5 | 42 |
| 105.8 | 415 | 13 |
| 107.7 | 428.5 | 14 |
| 109 | 430.5 | 65 |
| 113.2 | 445 | 29 |
| 120 | 468.5 | 29 |
| 121.2 | 472 | 34 |

during MIS 12c in the form of a short interval of high contribution of *G. crassaformis* sinistral, with peak values reaching 3% of the total foraminiferal assemblages at both sites.

4.2.2.3. Coiling direction of *Globorotalia truncatulinoides*. Changes in coiling direction of *G. truncatulinoides* are standard bioevents of the Pleistocene. They were initially used to correlate Late Pleistocene cores in the equatorial Atlantic ocean (Ericson and Wollin, 1968). More recently, the coiling direction of *G. truncatulinoides* has been used to reconstruct paleoceanographic changes in the North Atlantic Ocean since the Early Pleistocene (Billups et al., 2016, 2020; Kaiser et al., 2019). Abundance peaks of sinistral forms of *G. truncatulinoides*, or TE events, have been identified by Ducassou et al. (2018) in sediment cores

of the Gulf of Cadiz as remarkable biostratigraphic markers over the last 50 kyr.

At IODP Site U1386, MIS 1 is characterized by a single peak value of *G. truncatulinoides sinistral* ratio. This peak exceeds 87% at 9.1 kyr cal BP (Fig. 5) and corresponds to TE3 as described by (Ducassou et al., 2018). TE2 and TE1 were not observed in our records, likely due to low sampling resolution and a sedimentary hiatus corresponding to the last ~1.7 kyr BP.

During the MIS 12–11 interval, five peaks of *G. truncatulinoides sinistral* ratio exceeding 73% were identified and used to correlate IODP sites U1387 and U1386 (Fig. 6). The top two peaks occur during the transitions between MIS 11b and MIS 11c and MIS 11a and MIS 10. Two peak values exceeding 76% were also observed during MIS 11c. The bottommost “*G. truncatulinoides* event” (TE) with values ranging between 90 and 100% occurs during MIS 12b. During the MIS 11b, a TE event associated with a contourite level is observed at IODP Site U1386 but the corresponding bioevent and contourite bed are missing at IODP Site U1387 (Fig. 6). The most likely hypothesis to explain the lack of TE event and of contourite bed in sediment record from IODP Site U1387 during this period is a short coring gap between cores 339-U1387B-10 and 339-U1387B-11. Alternatively, both TE events and associated contourite beds, observed during the MIS 11c–MIS 11b interval at IODP Site U1386, could be condensated to a single TE event/contourite bed in the sedimentary record from IODP Site U1387 (Fig. 7). In all cases, this observation highlights an uncertainty about the age model of IODP Site U1387 during MIS 11b, which has been taken into account when interpreting the data.

5. Results

5.1. General sedimentological characteristics

The MIS 2–1 and MIS 12–11 intervals comprise several contourite beds characterized by high values of median grain size, sortable silt and percentage of sand (Figs. 7–8). The majority of contourite beds observed at IODP Site U1386 during the studied periods, are also present at IODP Site U1387, located 4 km further south-east, reflecting a remarkable spatial continuity. The silty to fine sand contouritic beds occurring during Heinrich Stadial 1 (HS1), the Younger Dryas and the Late

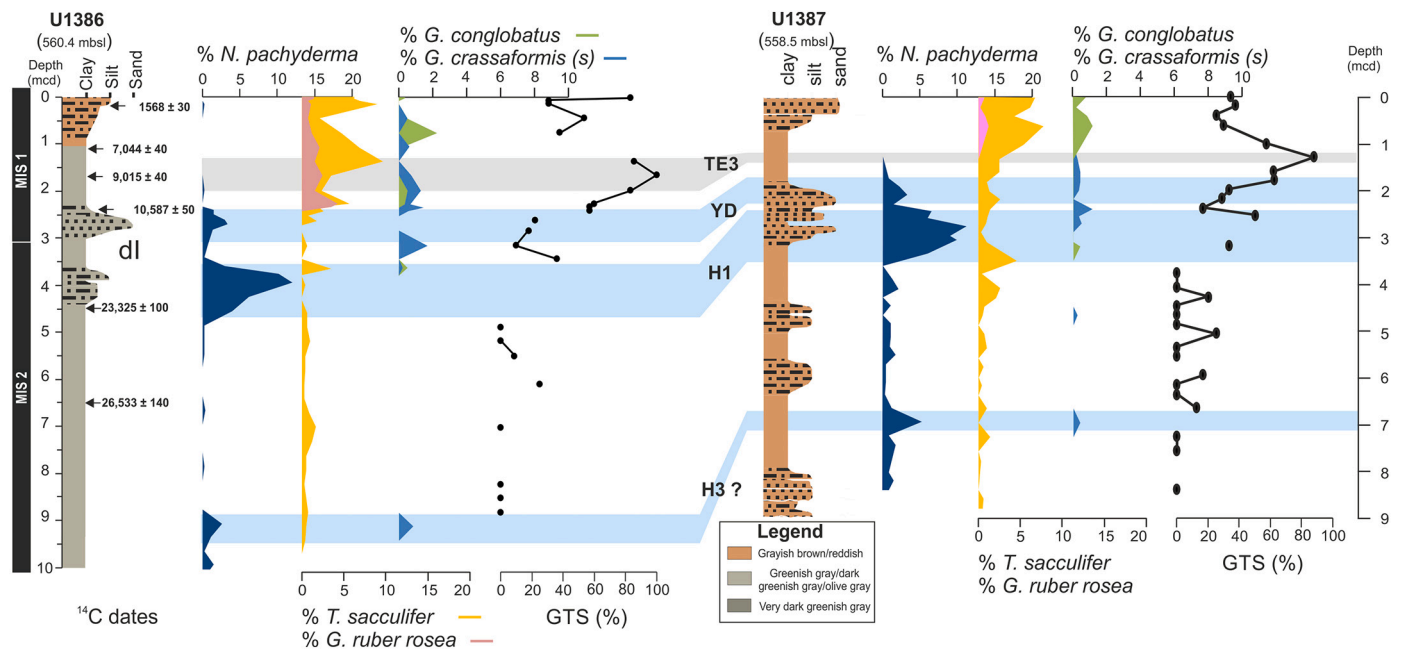


Fig. 5. Biochronology of IODP sites U1386 and U1387 during the MIS 2–1 interval. IODP Site U1386, from left to right: lithological log; radiocarbon dates and relative abundances of selected planktic foraminifera. IODP Site U1387, from left to right: lithological log; relative abundances of selected planktic foraminifera. MIS: Marine Isotope Stage; GTS: % *G. truncatulinoides* (s) ratio; YD: Younger Dryas; HS1 to HS3: Heinrich Stadials; mbsl: meter below sea level; mcd: meter composite depth. TE: *G. truncatulinoides* (s) event; dI: deglaciation I or transition between MIS 2 and MIS 1.

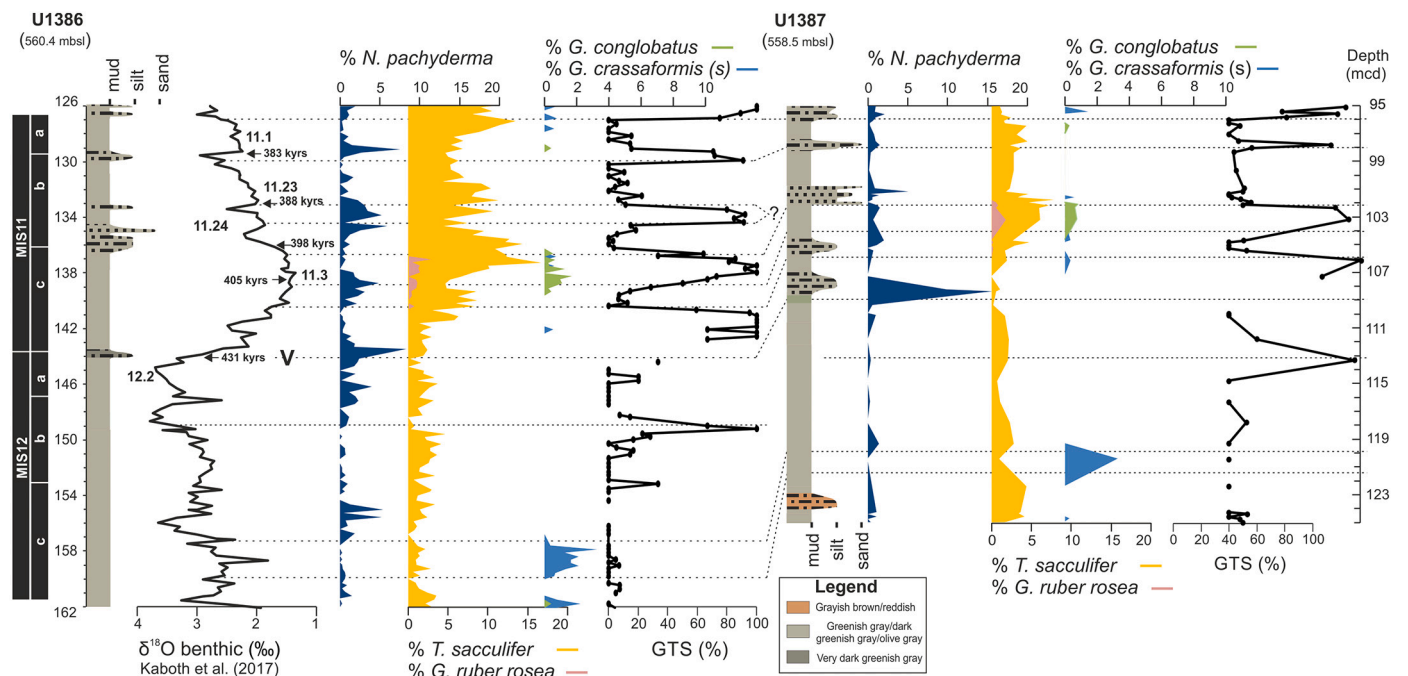


Fig. 6. Biochronology of IODP sites U1386 and U1387 during the MIS 12–11 interval. For IODP Site U1386, from left to right: stratigraphy from [Kaboth et al., 2017](#) with marine isotope events according to [Raisback et al. \(2015\)](#); lithological log; relative abundances of selected planktic foraminifera. For IODP Site U1387, from left to right: lithological log; relative abundances of selected planktic foraminifera. MIS: Marine Isotope Stage; GTS: % *G. truncatulinoides* (s) ratio; mcd: meter composite depth. dV: deglaciation V or transition between MIS 12 and MIS 11.

Holocene correspond, respectively, to peaks I, II and III described by [Faugeres et al. \(1986\)](#) in the Faro drift ([Fig. 7](#)). During the beginning of deglaciation V (Terminal Stadial Event 12.2; [Hodell et al., 2015](#)), the MIS 11c, the transition from substage MIS 11c to MIS 11b, MIS 11b, the transition from the substage MIS 11b to MIS 11a, and at the end of MIS 11a, contourite layers are fine-grained (muddy to silty contourites).

However, the analysis of grain size characteristics indicates that sediments in IODP Site U1387 are coarser than in IODP Site U1386, especially during MIS 11 and MIS 1. During MIS 12.2 and HS1, coarse quartz are present in sediments of IODP Site U1386 but not in sediments of IODP Site U1387 ([Figs. 7–8](#)).

Changes in carbonate content during the MIS 12–11 interval echo the

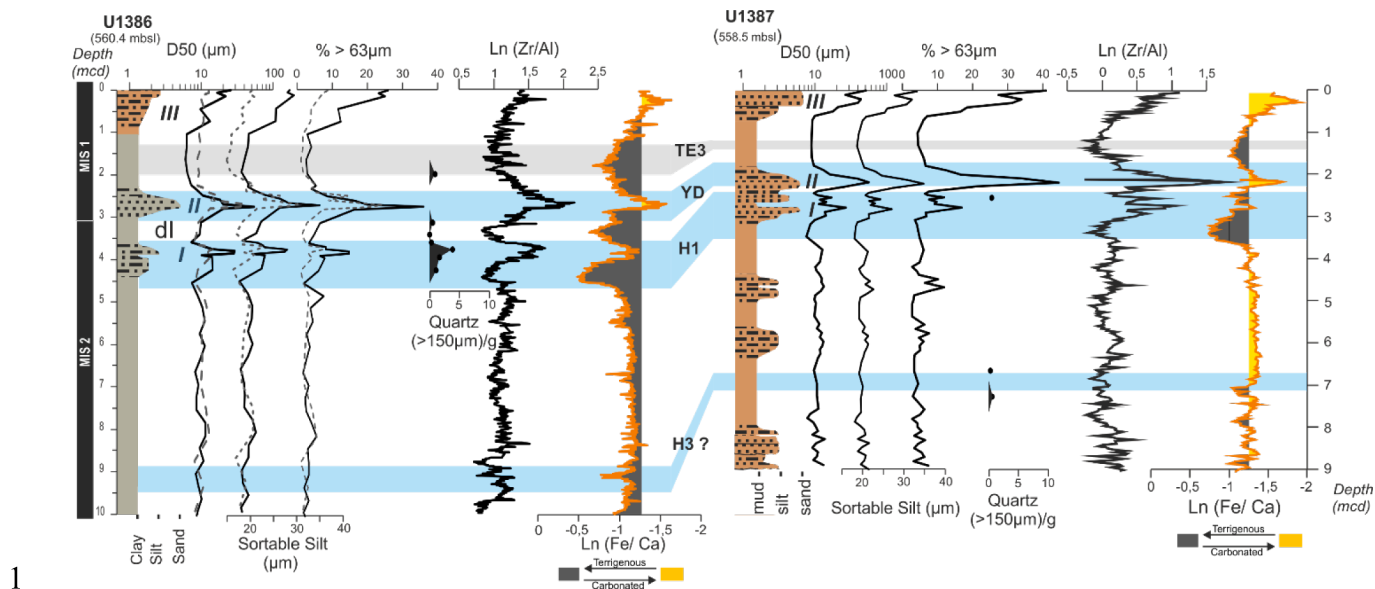


Fig. 7. Sedimentological features of IODP sites U1386 and U1387 during MIS 2-1 interval. IODP Site U1386, from left to right: lithological log resulting from visual description with contourite peaks (III, II and I) described by Faugeres et al. (1986); grain size characteristics of bulk (black line) and decarbonated (dotted line) sediment: median grain size (D_{50}); sortable silt; percentage of sand; number of quartz grains ($>150\mu\text{m}$)/g dry sediment; $\text{Ln}(\text{Zr}/\text{Al})$ and $\text{Ln}(\text{Fe}/\text{Ca})$ records. IODP Site U1387, from left to right: lithological log; median grain size (D_{50}); sortable silt; percentage of sand; number of quartz grains ($>150\mu\text{m}$)/g dry sediment; $\text{Ln}(\text{Zr}/\text{Al})$ and $\text{Ln}(\text{Fe}/\text{Ca})$ records. HS: Heinrich Stadials; YD: Younger Dryas; MIS: Marine Isotope Stage. III, II and I correspond to contourite peaks described by Faugeres et al. (1986); dl: deglaciation I or transition between MIS 2 and MIS 1.

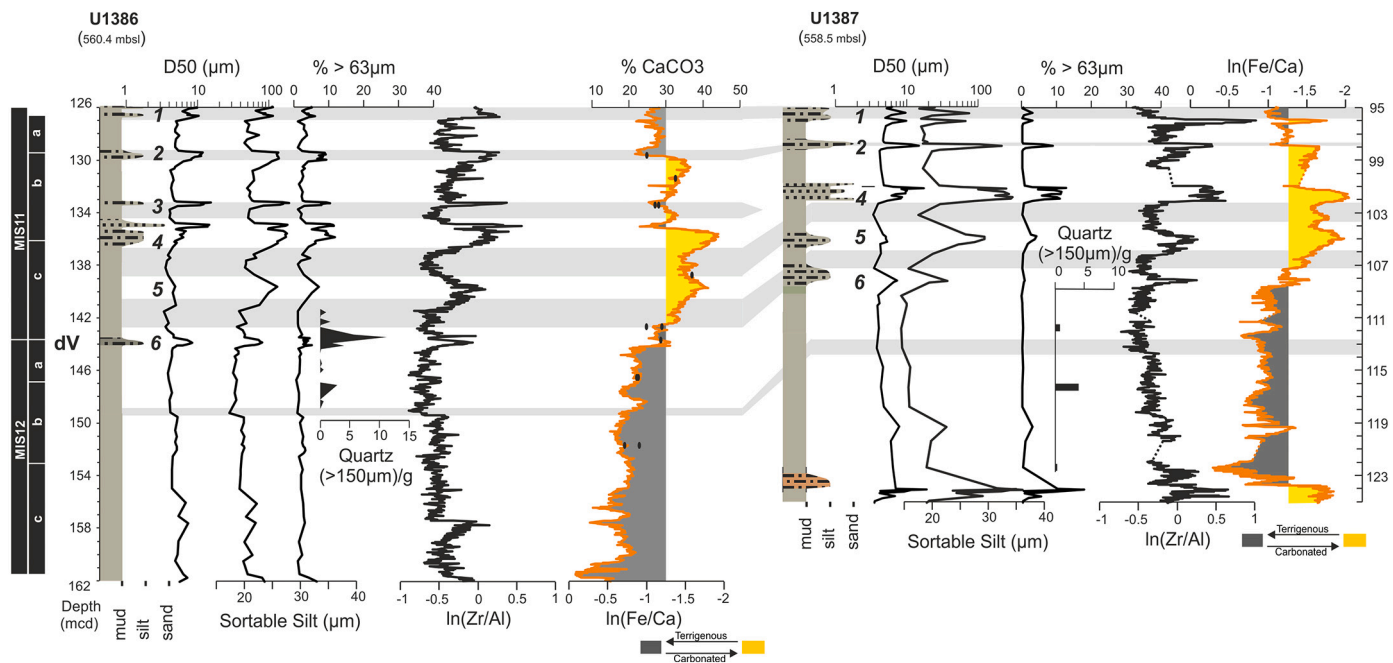


Fig. 8. Sedimentological features of IODP sites U1386 and U1387 during MIS 12-11 interval. For both sites from left to right: lithological log resulting from visual description with the identified contourite peaks 1-6; median grain size (D_{50}); sortable silt; percentage of sand; number of quartz grains ($>150\mu\text{m}$)/g dry sediment; $\text{Ln}(\text{Zr}/\text{Al})$ and $\text{Ln}(\text{Fe}/\text{Ca})$ records. Black dots: $\% \text{CaCO}_3$. 1-6 contourite peaks of MIS 12-11. MIS: Marine Isotope Stage. dV: deglaciation V or transition between MIS 12 and MIS 11. Grey rectangles: *G. truncatulinoides* events (TE).

Fe/Ca record (Fig. 8). Binocular and microscope observations indicate that carbonates particles are almost exclusively biogenic. The observed similarity between carbonate content and Fe/Ca ratio was used to estimate carbonate content from XRF-derived elemental ratios in other studied intervals. We therefore propose that the Fe/Ca ratio reflects changes in the relative contribution of biogenic vs. terrigenous components. Focussing on glacials, MIS 2 ($\text{CaCO}_3 \sim 25\text{--}30\%$) is more

carbonate-rich than MIS 12 ($\text{CaCO}_3 \sim 15\text{--}25\%$). Carbonate contents during MIS 11 and MIS 1 are higher (25-45%) than during glacials except during the Early Holocene (20-25%). Located farther from the coast, IODP Site U1387 shows overall higher carbonate contents than IODP Site U1386 during both, MIS 12-11 and MIS 2-1 (Figs. 7-8).

5.2. Sedimentary facies

Our detailed analysis of sedimentological features in IODP sites U1386 and U1387 complements the lithologies established during IODP Expedition 339 from smear slides (Stow et al., 2013), by revealing the occurrence of four main facies and ten subfacies (Fig. 9).

Facies A is represented by metric intervals of homogenous muddy sediment, and displays the finest grain size measured in our records with proportions of clays, silts and sands ranging from 75 to 90%, 9 to 24%, and less than 2%, respectively (Fig. 9). The D₅₀ is less than 5 μm with a unimodal distribution centered around 3–4 μm.

Facies B forms decimetric to multimetric intervals of silty-clay sediment and is the most abundant facies encountered in our records. The proportion of clays, silts and sands ranges from 44 to 80%, 18 to 51%, and 0 to 12%, respectively (Fig. 9), while the D₅₀ spans from 5 to 10 μm. Four subfacies within Facies B were identified according to grain size distribution and sediment composition. Subfacies B1 shows a bimodal grain size distribution with a principal mode ranging from 3 to 8 μm and a second mode ranging from 26 to 38 μm. Two compositional subgroups B1a (carbonate-rich) and B1b (terrigenous-rich) can be differentiated within subfacies B1 (Fig. 9). Subfacies B2 displays a unimodal grain size distribution and can be divided in two subgroups due to differences in modal curves and composition of sediment. B2a presents a unimodal modal curve centered around 8–12 μm with a variable proportion of carbonates (20–35%; Fig. 9). With coarser and carbonate-rich sediment (30–35%), B2b is characterized by a unimodal curve centered around 15–22 μm and slightly fine skewness (Fig. 9).

Subfacies B3 presents a bimodal distribution with two modes of grain size ranging from 4 to 8 μm and from 26 to 46 μm, and is principally composed of terrigenous sediment (Fig. 9). Subfacies B4 is characterized by a bimodal distribution with two well separated equal modes ranging from 3 to 6 μm and from 48 to 65 μm, and is more carbonate-rich (Fig. 9). This subfacies is the coarsest B facies with a significant proportion of sand (9–12%) and silt (32–43%). This facies can appear as the “mottled” facies described by Gonthier et al. (1984) in the Gulf of Cadiz.

Facies C consists of decimetric intervals of clayey-coarse silt sediment, and is composed of 29 to 46% of clays, 27 to 56% of silts and 11 to 27% of sands. Its D₅₀ varies between 15 and 21 μm. It presents a bimodal distribution with a dominant coarse mode ranging from 46 to 78 μm and a secondary fine mode ranging from 3 to 9 μm. This facies is also characterized by a mesokurtic grain size distribution and a fine-tail skewness (Fig. 9). The composition of sediment allows to differentiate two subgroups: a terrigenous subfacies (Ca) and a carbonate-rich subfacies (Cb) (Fig. 9).

Facies D is composed of very thin (centimetric) carbonate-rich silty-sand beds representing the coarsest sediments observed in our archives. The proportion of clays, silts and sands ranges from 16 to 25%, 38 to 44% and 31 to 45%, respectively. D₅₀ ranges from 49 to 57 μm and the grain size distribution shows a principal mode between 66 and 78 μm. This facies is also characterized by leptokurtic grain size distribution and a very fine-tail skewness (Fig. 9).

5.3. Sedimentary sequences of contourite beds

The gradual facies succession during the periods studied at IODP sites U1386 and U1387 allowed the definition of three sequences (Fig. 10 and Table 4). They are composed of coarsening-up and a fining-up sub-sequences, except Holocene sequences which present only a coarsening-up sequence (Sequence 2b, Fig. 10). The thicknesses of coarsening-up and fining-up sub-sequences varies between 63 and 299 cm, and 15 and 203 cm, respectively. We interpret these vertical sequences and their associated grain size variations as an increase and then a decrease of bottom-current velocity. At this location in the Gulf of Cadiz, beds with such sequences are considered to be contourite layers formed by the MOW_U (Faugères et al., 1984; Gonthier et al., 1984).

Sequence 1 is the finest sequence encountered in our records and is characteristic of muddy contouritic beds. The increase within this sequence of percentage of silts, its zero or low skewness, its symmetrical distribution of the coarsest facies (B) and the progressive contact between facies are compatible with very limited bottom current increase

| Facies | Grain size | Modal Curves | Sand (%) | Silt (%) | Clays (%) | Mode (μm) | Skewness | Kurtosis | General composition (%CaCO ₃) | Complete lithologic name (Stow et al., 2012) |
|------------|--------------------|--------------|----------|----------|-----------|--|----------------------|------------------------|---|--|
| Facies A | Muddy | | 0-2 | 10-24 | 75-90 | Unimodal :4 | Low skewness | Platycurtic/Mesocurtic | Terrigenous (15-30%) | Calcareous mud |
| Facies B1a | Silty-clay | | 2-5 | 24-39 | 57-75 | Principal mode :3-6 Secondary mode :38-45 | Coarse tail skewed | Platycurtic | Terrigenous (15-25%) | Nannofossils ooze with mud |
| Facies B1b | | | 0-4 | 18-30 | 67-80 | Principal mode :3 Secondary mode :26-35 | Coarse tail skewed | Platycurtic/Mesocurtic | Carbonate rich (30-40%) | Nannofossils/calcareous silty mud |
| Facies B2a | | | 1-5 | 33-44 | 52-62 | Unimodal :7-12 | Symmetrical | Platycurtic | Terrigenous (20-30%)* | |
| Facies B2b | | | 2-12 | 37-51 | 44-55 | Unimodal :15-22 | Slightly fine skewed | Platycurtic | Carbonate rich (30-35%) | |
| Facies B3 | Silty-clay | | 2-12 | 23-43 | 50-75 | Bimodal : 3-6 / 26-45 | Symmetrical | Platycurtic | Terrigenous (20-30%) | Silty-mud with biogenic carbonates |
| Facies B4 | | | 9-12 | 32-43 | 45-59 | Bimodal : 3-6 / 48-65 | Symmetrical | Platycurtic | Carbonate rich (>30%) | |
| Facies Ca | Clayey coarse-silt | | 11-27 | 29-56 | 26-46 | Principal mode :45-78 Secondary mode :3-7 | Fine skewed | Mesocurtic | Terrigenous (20-30%) | Sandy-mud with biogenic carbonates |
| Facies Cb | | | | | | | | | Carbonate rich (30-35%) | Silty-muddy calcareous ooze |
| Facies D | Silty-sand | | 31-45 | 38-44 | 16-25 | Principal mode :65-78 | Very fine skewed | Leptocurtic | Carbonate rich (>35%) | Sandy-silt with biogenic carbonates |

Fig. 9. Summary of sedimentary facies identified in IODP sites U1386 and U1387. Yellow: CaCO₃ content >30%; Grey: CaCO₃ content <30%. *: carbonate content of Facies B2b can be slightly more carbonate rich (35%). (For interpretation of the references to colour in this figure legend, the reader is referred to the web version of this article.)

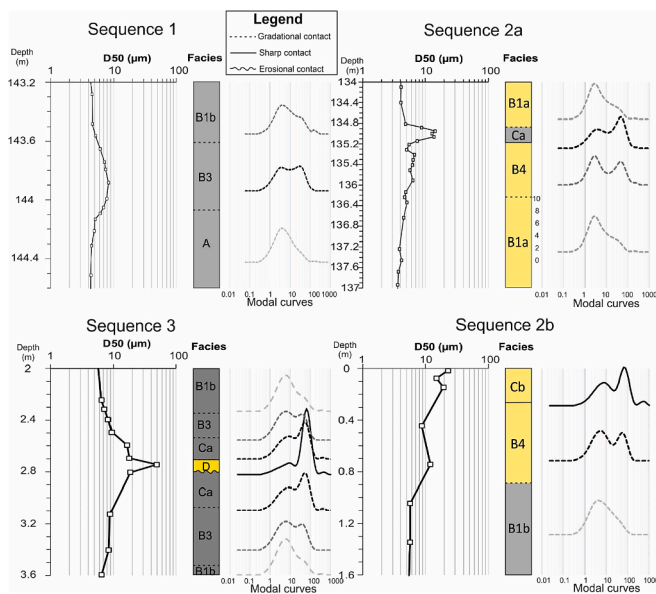


Fig. 10. Detailed sedimentological description of sedimentary sequences 1, 2 (a and b) and 3. A, B (1,2,3 and 4), C, D represent sedimentary facies described in the main text. Yellow: CaCO₃ > 30%; Grey: CaCO₃ < 30%. (For interpretation of the references to colour in this figure legend, the reader is referred to the web version of this article.)

(< 10 cm s⁻¹) (Pepple, 2020). We discriminate two types of muddy contourite beds composing Sequence 1 according to their composition and grain size characteristics: a terrigenous one (A-B3-B1b) during dV and a carbonate-rich one (B1a-B4-B1a) during MIS 11 (Fig. 8 and Table 4).

Sequence 2 is a medium grain size sequence typical of silty contouritic beds, and corresponds to the “Sequence 1” described by Toucanne et al. (2007) during Dansgaard-Oeschger events in sediments cores of the Gulf of Cadiz beneath the path of MOW_U. The dominance of silts, a fine skewness, and a mesocurtic distribution of the coarsest facies (C) within this sequence suggest, according to Brackenridge et al. (2018) deposit induced principally by a weak current (10–15 cm s⁻¹). In addition, the sharp contact between Facies B and C indicates that Sequence 2 recorded a higher current speed than Sequence 1. Three types of silty contourite beds composing Sequence 2 were recognized based on their composition and grain size characteristics: (1) terrigenous beds (B2-B3-Ca-B3-B1b) observed during HS1, and (2) Holocene carbonate-rich beds (B1b-B4-Cb) (Fig. 8 and Table 4), both sequences showing synchronous increases in granularity and carbonate content (Fig. 10); the third type of silty contouritic beds, more atypical, presents (3) a sequence of carbonate-rich coarsening-up trend, followed by a more terrigenous maximum of grain size, and ending with carbonate-rich fining-up sediments (B1a-B4-Ca-B1a; Fig. 10 and Table 4). This last special sequence is observed during MIS 11 at both site U1386 and U1387 (Table 4).

Table 4

Summary table of the sequences observed in our records. Normal cruces: at IODP Site U1386. Underlined cruces: at IODP Site U1387. MIS: Marine Isotope Stage; YD: Younger Dryas; HS: Heinrich Stadial; dV: deglaciation V or transition between MIS 12 and MIS 11.

| Sequence | Facies succession | U1386 - U1387 | | | | | Interpretation |
|----------|----------------------|---------------|--------|-------|-------|-------|---|
| | | Holocene | MIS 11 | YD | HS 1 | dV | |
| 1 | A-B3-B1b | | | | | X - X | Weak (<10 cm.s ⁻¹) Terrigenous Carbonate-rich |
| | B1a-B4-B1a | | X - X | | | | |
| | B2a/B2b-B3-Ca-B3-B1b | | | | X - X | | |
| 2 | B1a-B4-Ca-B1a | | X - X | | | | Medium (10–15 cm.s ⁻¹) Change from carbonate-rich to terrigenous Carbonate-rich |
| | B1b-B4-Cb | X | | | | | |
| | B2a-Cb-D | X | | | | | |
| 3 | B1b-B3-Ca-D-B3-B1b | | | X - X | | | Strong (15–25 cm.s ⁻¹) Carbonate-rich Terrigenous |

Sequence 3 is the coarsest sequence encountered in our records and is characteristic of fine sand contouritic beds. It presents strong similarities with “Sequence 2” proposed by Toucanne et al. (2007) during the Younger Dryas within a sediment core under the influence the MOW_U. A similar proportion of sand and silt, a very fine skewness and a leptokurtic distribution of the coarsest facies (D) within this sequence indicate, as proposed by (Brackenridge et al., 2018), a deposit affected by progressive winnowing at higher current speeds (15–25 cm.s⁻¹). We observe two types of fine sand contouritic beds based on their composition and the contact between individual facies: (1) terrigenous beds (B1b-B3-Ca-D-B3-B1b), characterized by an erosional contact between the Facies Ca and D, and observed during the YD (Fig. 10); (2) Holocene carbonate-rich beds (B2a-Cb-D) observed only at IODP Site U1387 (Table 4) and which present a sharp contact between facies Cb and D. Both types of contourite beds present simultaneous increases and decreases of granularity and carbonate content.

6. Discussion

6.1. Understanding grain size information: Current velocity and sediment supply over the Faro drift

6.1.1. Bottom current indicators and MOW velocity in the Gulf of Cadiz

A majority of paleoceanographical studies in the Gulf of Cadiz used the weight percentage of sands (>63 µm) as an indicator of the intensity of the MOW flow strength (e.g. Rogerson et al., 2005; Llave et al., 2006; Voelker et al., 2006; Kaboth et al., 2017). MOW velocity has also been estimated using the mean of the fine grain size fraction (<63 µm; Voelker et al., 2006, 2015a), the 90th centile (D₉₀; Hanquiez et al., 2007), the sortable silt (Toucanne et al., 2007), or by using the median grain size (Toucanne et al., 2007; Ducassou et al., 2018). Based on a geochemical approach Bahr et al. (2014) showed that the ln(Zr/Al) ratio reflects bottom current velocity in the Gulf of Cadiz, establishing this ratio as an indicator of MOW flow strength (Bahr et al., 2015; Voelker et al., 2015a). More recently, Brackenridge et al. (2018) and Pepple (2020) used different grain size parameters as the median, the sorting, and the skewness and kurtosis to reconstruct bottom current speed in the Gulf of Cadiz.

In addition to current velocity, other factors such as changes in sediment supply or depositional processes such as turbidity currents can influence sediment texture (Stow et al., 1986). Among these factors, the biasing effect of sediment supply changes upon proxy records of bottom current velocity is barely considered. The sources of sediments to the Faro drift are mainly carbonate skeletons of primary and secondary producers, and terrigenous material delivered by South-West Iberian rivers (e.g., Alonso et al., 2016). In the following discussion we compare the facies succession established in this study with different bottom current indicator signals in order to have a better understanding of their meanings in the Faro drift.

We find that the sortable silt is sensitive to slight variations of bottom current velocity of less of 10 cm.s⁻¹ (Facies B3 and B4; Brackenridge et al., 2018). However, this grain size parameter can present identical

values for Facies B and C or/and C and D (Fig. 11), thus demonstrating that the sortable silt can be limited in the accurate reconstruction of bottom current exceeding 10–15 cm.s⁻¹. In contrast, the D₅₀ does not always clearly react with minor increases of MOW_U velocity (Facies B3 and B4) but instead reliable records medium current speeds (>10–15 cm.s⁻¹).

To reduce the bias caused by changes in sediment supply (foraminiferal or IRD abundances and downslope supply) on the velocity information inferred by the weight percentage of sands, some authors generally take into account the 63–150 μm fraction only (Rogerson et al., 2005; Kaboth et al., 2016, 2017, Sierro et al., 2020). Our results show that sand contributions derived from wet sieving (weight % sand) display significant discrepancies from laser granulometry-derived values (Fig. 11): weight % sand underestimates the amount of sand in the sediment, especially when the sand is terrigenous and mica-rich. Moreover, the weight % sand (>63 μm and 63–150 μm) present more

similarities with downcore profiles of planktic foraminiferal abundance than with gradual facies succession (Fig. 11). These observations suggest that the weight of the coarse fraction reflects both changes in bottom current velocity and changes in the flux of calcareous shells to bottom sediments (Fig. 11).

Representing the relative enrichment of heavy minerals over less dense aluminosilicates under the influence of bottom current flow, the Zr/Al ratio (Bahr et al., 2014) provides a high resolution record of bottom current velocity. This elemental ratio presents similar values between silty-clay facies (B3) of HS1 and YD and clayey coarse-silt facies (Cb) at IODP Site U1386 (Fig. 11). Both facies are principally controlled by the maximum carrying capacity of the current but Facies B3 is normally influenced by a weaker current velocity than facies Cb (Brack-enridge et al., 2018). Similarly, at IODP Site U1387 the coarse-silt facies (Ca) of HS1 and YD has ln(Zr/Al) values comparable to those of the silty-sand facies (D) of the Holocene. However, the facies D deposit is affected

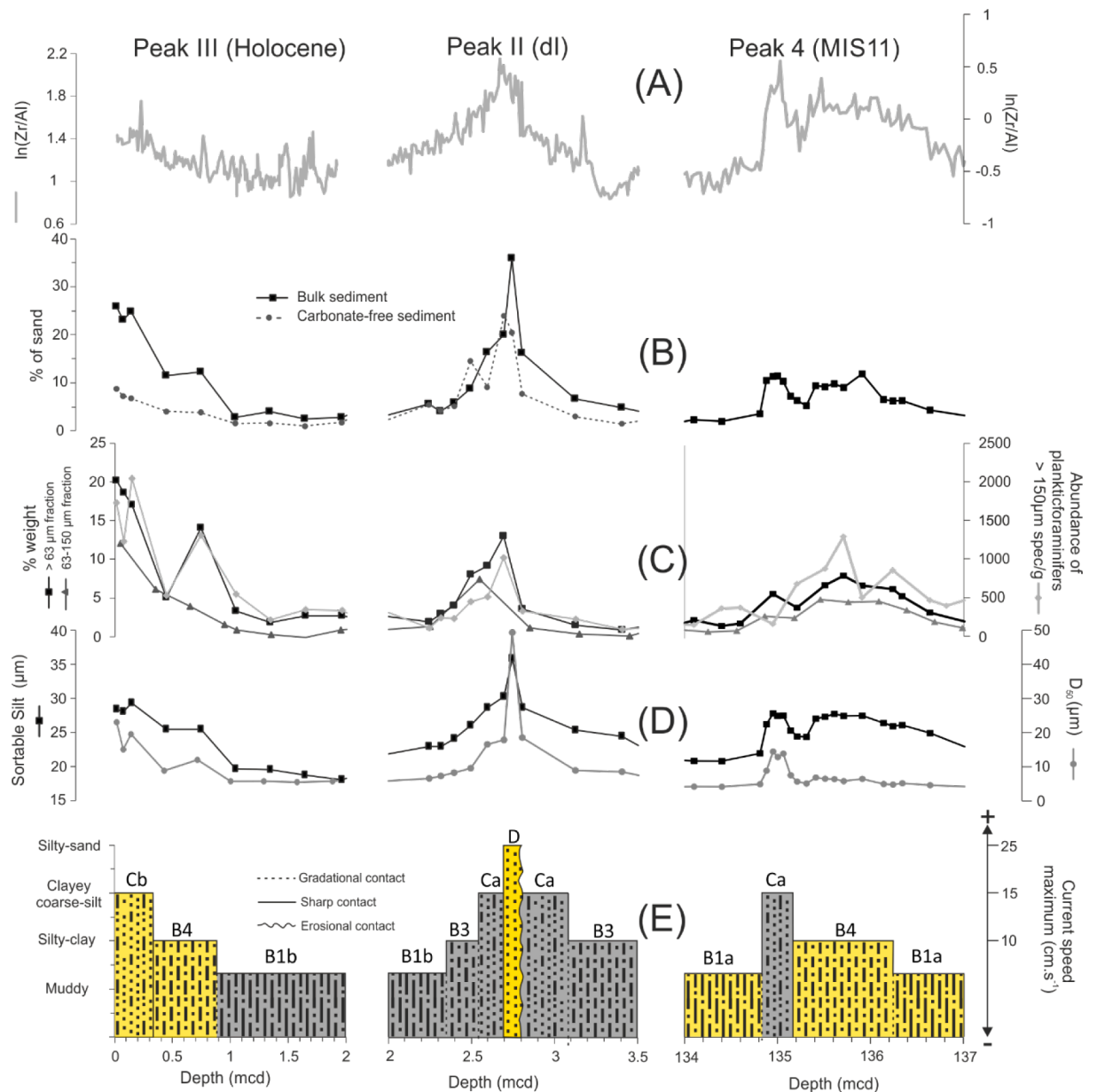


Fig. 11. Close-up of the most recent contourite beds of the Faro drift. From left to right: contourite beds (peaks) III, II and 4. From top to bottom: (A) ln(Zr/Al) ratio; (B) % of sand fraction (particles >63 μm) in bulk (black symbols) and carbonate free sediment (dark grey symbols); (C) weight % of the >63 μm (black symbols) and 63–150 μm fractions (dark grey symbols; Kaboth et al., 2017) and abundance of >150 μm planktic foraminiferal tests (light grey); (D) sortable silt (dark grey symbols) and D₅₀ (black symbols); (E) facies succession and associated current speed.

by non-deposition or progressive winnowing at higher current speeds ($15\text{--}25\text{ cm s}^{-1}$; Pepple, 2020), whereas the facies Ca is not impacted by such high current velocities ($10\text{--}15\text{ cm s}^{-1}$; Brackneridge et al., 2018). The “coarse” material available being generally more carbonate-rich during the Holocene, the Zr/Al ratio probably slightly underestimate the MOW_U speed during this period.

In the absence of evidence of turbidite events in the Faro drift area during the studied period (e.g. Gonthier et al., 1984; Hernández-Molina et al., 2003), we relate the vertical distributions of contourite facies at IODP sites U1386 and U1387 during the MIS 12–11 and MIS 2–1 intervals to variations in bottom current velocity.

6.1.2. Impact of changes in sediment supply: Example of a contouritic sequence of the MIS 11

Unlike most of contourites described in the Faro drift during the MIS 1 (e.g. Gonthier et al., 1984; Stow et al., 1986) the coarsest part of the MIS 11 contourite sequences does not correspond to maxima in carbonate content (Fig. 11). While the increase of current allows the deposition of carbonate silty particles (facies B4) which is mainly controlled by the carrying capacity of the current, the considerable increase of terrigenous particles in the study area suggests a change in sediment supply. This assumed change in terrigenous sediment delivery to Faro drift during MIS 11 is concomitant with an increase of % *N. pachyderma* reflecting the decrease of sea-surface temperatures (SST) which corresponds to Heinrich-type ice-rafting events (Ht) 2 and 3 detected in Iberian margin records during MIS 11 (Rodrigues et al., 2011; Oliveira et al., 2016). This drop of SST along the Iberian margin has strongly negatively impacted the primary productivity (coccolithophore productivity) and thus the production of secondary producers alike planktic foraminifera during Ht2 and Ht3 (Cavaleiro et al., 2020). The terrigenous biomarkers from southwest Iberian margin indicate, in turn, a very slight decline (Rodrigues et al., 2011), during the corresponding relatively dry hinterland conditions (Oliveira et al., 2016). These changes in terrigenous and biogenic sediment input in the Faro drift coincide with the strongest current velocity recorded in these sequences which probably triggered both the winnowing or the non-deposition of terrigenous fine particles and sand sediment supply by saltation. The decrease of carbonate content during the current velocity maxima indicates however, that the increase in terrigenous sediment supply compared to the carbonate supply, such as medium MOW_U velocities, has an influence on sedimentation. Consequently, changes in sediment supply, particularly those induced by changes in productivity vs. export of terrigenous particles can play an important role on the facies succession and contourite sequences in the Gulf of Cadiz (Fig. 11).

6.2. Behaviour of the branches of the MOW during MIS 12–11 and MIS 2–1

6.2.1. Glacials

The finest facies (A, B1a and B2) identified at IODP sites U1386 and U1387 characterize sediments of MIS 12 and MIS 2 ages. This clay and silty-clay dominated sedimentation as well as the absence of contourite sequences in the studied cores confirm previous studies (Hanquiez, 2006; Llave et al., 2006) which suggest a reduced MOW_U activity during glacials. This reduced activity coincides, during MIS 2, with a deeper circulation of the MOW (e.g., Schönfeld and Zahn, 2000) as well as a strengthening of the lower branch (MOW_L). This strengthening is particularly active during HE 2 and HE 3 as shown by the generation of coarse contouritic beds (Llave et al., 2006; Voelker et al., 2006; Toucanne et al., 2007). This general pattern (deeper circulation of the MOW) was probably enhanced during MIS 12 which was characterized by an exceptionally low sea level as well as some of the coldest and driest climate conditions of the Late Pleistocene in the Western Mediterranean region (Sánchez Goñi et al., 2016).

While being both dominated by muddy or silty-clay, U1386 and U1387 sediments of MIS 12 and MIS 2 ages show conspicuous facies

discrepancies in-between the two glacials or in-between sites. The MIS 2 facies B2 shows a different modal distribution and a generally higher carbonate concentration than the MIS 12 facies A and B1a. We interpret these differences as an indication of changes in sediment supply between these periods. The extremely low sea-level (-30 m relative to MIS 2) during MIS 12 (Waelbroeck et al., 2002; Rabineau et al., 2006) has contributed to the high export of detrital particles to the middle slope (Mestdagh et al., 2019), and their accumulation in the Faro drift via their redistribution by the MOW. During MIS 12, the apparent mismatch between records of $\ln(\text{Fe}/\text{Ca})$ in IODP Site U1386 and biomarkers in a marine core of the southwestern Portuguese margin (MD03-2699), suggests a minor role of coccolithophore productivity and continental inputs (Rodrigues et al., 2011) on the sedimentation in the Faro drift during this glacial stage.

MIS 12 sediments at IODP sites U1386 and U1387 are characterized by two successive facies, from silty-clay sediment (B1a) at the base of this interval to muddy (A) sediment for the youngest part. This vertical transition to a less coarser facies may reflect a MOW_U deepening during MIS 12, and thus a weaker influence of the bottom current on the sedimentation in the Faro drift.

Interestingly, the carbonate content in sediments of IODP Site U1387 is generally higher than in IODP Site U1386 records. Fine detrital particles, which have mainly a southwestern Iberian origin (Guadalquivir River; Alonso et al., 2016), are redistributed in the Faro drift by the MOW. Consequently, IODP Site U1387, the furthest site from the core of MOW_U , is likely to be less supplied in terrigenous fine particles than IODP Site U1386, explaining the discrepancy in carbonate content between both sites.

6.2.2. Deglaciations

Based on the presence of a coarse contouritic bed in the Faro drift, (“peak I” after Faugeres et al. (1986)), many authors argued for an active circulation of the MOW during HS1 (e.g. Mulder et al., 2002; Rogerson et al., 2005; Llave et al., 2006; Voelker et al., 2006; Ducassou et al., 2018). This strengthened flow through the Strait of Gibraltar has been related to the more active formation of WMDW in the Gulf of Lion during Heinrich and stadial events (Rohling et al., 1998; Cacho et al., 2000; 2006; Sierro et al., 2005; Frigola et al., 2008; Bassetti et al., 2010). Our results, in agreement with previous works (Hanquiez, 2006; Llave et al., 2006; Ducassou et al., 2018), show a considerable increase in MOW_U activity (Seq2a) which coincides with an enhanced MOW_L flow (Mulder et al., 2002; Rogerson et al., 2005; Llave et al., 2006; Voelker et al., 2006; Toucanne et al., 2007; Ducassou et al., 2018). Following Hanquiez (2006), we propose that MOW circulation increased in the Gulf of Cadiz during HS1, and that the lower branch was more active than the upper one. Change in sediment supply plays an important role on the vertical succession of facies during HS1. The youngest part of MIS 2 is characterized by a high contribution of terrigenous particles to sediments of the Faro drift system. Such an accumulation is due to the high export of detrital particles to the slope during this low sea-level interval, as supported by a stratigraphical study on the continental margin of the northern Gulf of Cadiz (Mestdagh et al., 2019). The proximity of river mouths, as well as the downslope transport in the nepheloid layer and the redistribution by the MOW, may have favoured the high contribution of terrigenous particles to the sedimentation of the Faro drift (Stumpf et al., 2011).

Early on, MOW_U strengthening allowed the deposition of terrigenous silty particles (facies B3) controlled principally by the maximum carrying capacity of the current. Then, with a progressive increase in MOW_U velocity, sediment accumulation was affected by winnowing. Saltation might also have contributed to the coarse sedimentation recorded at the end of MIS 2, bringing quartz from upstream turbidites deposits during a period of low sea-level ($-130\text{--}-110\text{ m}$ compared to modern sea-level; Waelbroeck et al., 2002; Elderfield et al., 2012). The rise of carbonate content during this coarsening indicates that winnowing of fine terrigenous particles dominated over the supply of

detrital sand by saltation.

The YD presents the coarsest contourrite sequence (Seq 3) identified over the studied periods at IODP sites U1386 and U1387. This sequence contains an erosional contact between facies Ca and D (Fig. 9). Seq3 might be seen as an analogue to coarse contourrite beds of YD age recorded in cores under the influence of MOW_L (Mulder et al., 2002;

Rogerson et al., 2005; Llave et al., 2006; Voelker et al., 2006; Toucanne et al., 2007) and known as “Peak II” (Faugeres et al., 1986). We interpret the more carbonate-rich composition of the YD contouritic beds compared to the HS1 beds as induced by a stronger winnowing of the fine terrigenous particles due to high bottom current velocities. A change in terrigenous input has also to be considered since, unlike the

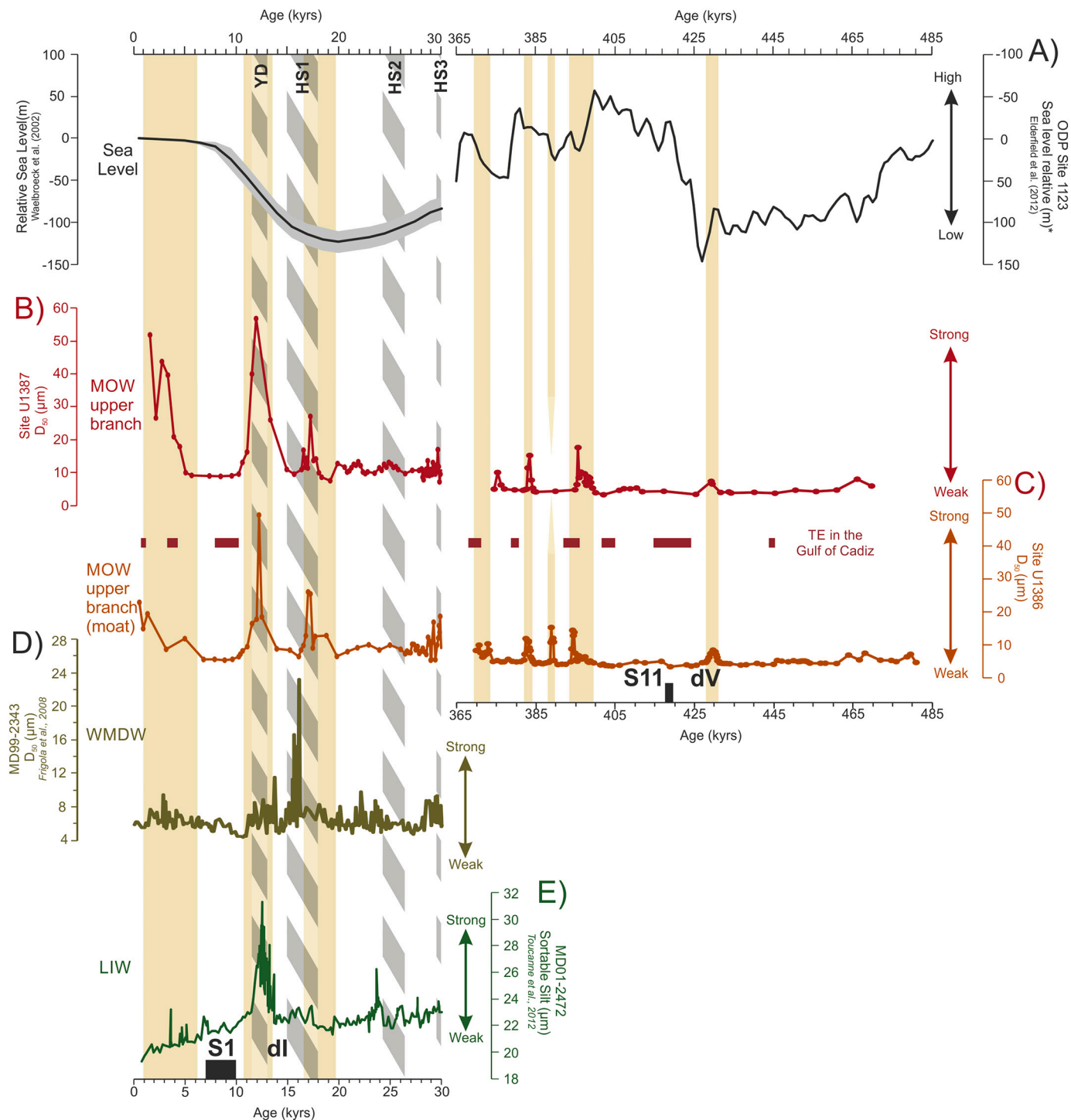


Fig. 12. Upper Mediterranean Outflow Water (MOW_U) flow strength and paleoclimatic context. A: eustatic level after Waelbroeck et al. (2002)(left) and Elderfield et al. (2012) (right). B-C: mean grain size (D_{50}) reflecting MOW_U velocity at the sea floor at IODP sites U1386 and U1387. D: mean grain size (D_{50}) of core MD99-2343 collected on the drift of Minorca Islands, approximating Wester Mediterranean Deep Water (WMDW) flow speed (Frigola et al., 2008). E: sortable silt (SS) of core MD01-2472 indicating the Levantine Intermediate Water current intensity along the eastern margin of Corsica (Toucanne et al., 2012). MIS: Marine Isotope Stage; YD: Younger Dryas; HS: Heinrich Stadials; dV(I): deglaciation V(I) or transition between MIS 12(2) and MIS 11(1); V: *G. truncatulinoides* (s) Events; S: sapropel.; Yellow rectangles: contourrite beds. (For interpretation of the references to colour in this figure legend, the reader is referred to the web version of this article.)

HS1 deposits, the YD contourite beds do not contain any coarse quartz (>150 μm). Differences in sea level between these periods (Fig. 12) likely explain the reduced coarse and fine terrigenous particles input in the more distal Faro drift during the YD. Despite a reduction in detrital sediment supply, the coarseness of facies D as well as the presence of an erosional contact within Seq3 point to the highest velocities of the MOW_U during the YD (Fig. 9). The YD is thus characterized by an enhanced circulation of the lower and upper branches of the MOW as proposed by Hanquiez (2006). The rise in sea level associated with the particularly active circulation of the LIW in the Mediterranean Sea (Toucanne et al., 2012) probably favoured enhanced circulation of the two branches of the MOW during this cold inception (Fig. 12).

The contourite beds (Seq1) observed during the transition from MIS 12 to MIS 11 reflects high activity of the MOW_U . Its limited amount of coarse material compared to HS1 (Seq2), a period when sea level was similar to the MIS 12–MIS 11 transition (Waelbroeck et al., 2002; Elderfield et al., 2012), suggests though that MOW_U activity and/or terrigenous supply were lower during dV than during the final part of MIS 2 (Fig. 12).

6.2.3. MIS 11 and MIS 1

The presence in our sedimentary records of contourite beds of varying coarseness underscores the enhanced activity of the MOW_U during MIS 11 and MIS 1 (Fig. 12) as suggested by Rogerson et al. (2005), Llave et al. (2006), Bahr et al. (2014), and Kaboth et al. (2016).

During the MIS 11 and Holocene high-sea level periods, contourite beds are coarser and more carbonate-rich at IODP Site U1387 which is located at a greater distance from the moat, than at IODP Site U1386. Two factors can be put forward to explain these spatial compositional and grain size discrepancies: differences in bottom current speed due to intensification and/or spatial variability of the MOW_U , and/or differences in sediment supply. When located higher in the water column, the core of the MOW_U has a greater influence at IODP Site U1387 during MIS 11 and MIS 1 because of its slightly shallower position than at IODP Site U1386. When sea level is lower, especially at the beginning of deglaciations (dV, HS1), the core of the current migrates downwards, affecting both U1386 and U1387. During MIS 11 and MIS 1, deposition of fine terrigenous particles in the studied area has been limited by (1) the high sea-level (Waelbroeck et al., 2002) which favoured the deposition of a portion of detrital clays in the continental shelf and prevented the export of terrigenous particles to the middle slope and (2) the active MOW_U which limited the deposition of fine particles, in particular during its strengthening. These findings are supported by the overall higher sedimentation rates during glacial intervals than during interglacials in the Faro drift (Kaboth et al., 2017).

The “Peak III” coarse contourite bed described by Faugeres et al. (1986) and many authors in the Faro drift (e.g., Mulder et al., 2002; Llave et al., 2006) and observed at IODP sites U1386 and U1387, is also recorded in our archives during the Holocene. It reflects a slight intensification of the MOW_U around 6 kyrs cal BP and then a considerable strengthening of the flow over the last 3 kyrs (Fig. 12). These accelerations of the MOW_U are probably due to the renewed ventilation of the LIW 6 kyrs ago (Toucanne et al., 2012) and a strengthened deep-water formation (WMDW) 4 kyrs ago in the Gulf of Lion (Frigola et al., 2008).

Our results show that Peak III dating from the end of Holocene is much coarser than the contouritic beds encountered in MIS 11. The increases of MOW_U flow strength during the transition from the interglacial (MIS 11c) to the following glacial (MIS 10), took place while sea level was more or less similar to the Holocene sea level (Waelbroeck et al., 2002; Elderfield et al., 2012). Moreover, during both periods relatively higher primary productivity and associated secondary production of foraminifera have been observed south-west off the Iberian peninsula (Rodríguez et al., 2009, 2011). Consequently, despite similarities in the sedimentary processes, the difference of coarseness of contourite beds between both MIS 11c and MIS 1 suggests that MOW_U velocity was higher during the end of Holocene than during MIS 11

despite no evidence of sequence finning-up.

The MIS 11 sedimentary hiatus observed in the MOW_L -influenced IODP Site U1390 corresponds to the Late Quaternary Discontinuity in the south Portuguese CDS, which is related to tectonic activity and uplift-induced erosion (Hernández-Molina et al., 2016; Lofi et al., 2016). However, the possibility that this hiatus was also induced by a contemporary strengthening of MOW_L can not be ruled out. Indeed, the benthic foraminiferal assemblages described in sediments of IODP Site U1391 off south-west Portugal indicate that MOW_L reached its highest intensity of the last 900 ka during MIS 11 (Guo et al., 2017). These results highlight a slightly different flow pattern of the MOW between MIS 11 and MIS 1. While the most recent interglacial is characterized by an intense MOW_U flow (Rogerson et al., 2005; Llave et al., 2006; Bahr et al., 2014; Kaboth et al., 2016) and a less active MOW_L circulation (Mulder et al., 2002; Rogerson et al., 2005; Llave et al., 2006; Voelker et al., 2006; Toucanne et al., 2007), our results indicate that MOW_U circulation during MIS 11 was lower while the MOW_L circulation was particularly intense.

A relationship between sapropel formation in the Eastern Mediterranean Basin and low MOW activity was first demonstrated for Sapropel 1 (S1) during the Holocene (Voelker et al., 2006; Toucanne et al., 2007; Rogerson et al., 2012; Kaboth et al., 2016). It was then extended for all sapropels down to MIS 7 (Sierro et al., 2020). Our results confirm the low activity of the MOW_U during S1 and highlight a reduced MOW_U flow during S11 (418.9 kyrs cal. BP; Konijnendijk et al., 2014; Fig. 12).

6.3. MOW strengthening during deglaciation V and MIS 11: A strong influence on North Atlantic climate?

Model simulations suggest that the AMOC is significantly influenced by the contribution of the MOW (Reid, 1979; Rahmstorf, 1998; Ivanovic et al., 2013; Wu et al., 2007) but the effects of Mediterranean water masses on AMOC remain unclear (Swingedouw et al., 2018). Indeed, while a strengthening of MOW does not influence North Atlantic Deep Water production (NADW; Khélifi et al., 2014), it stimulates the shallow branch of AMOC (Bahr et al., 2015; Sarthein et al., 2018). Sediment records have shown a negative feedback between exchanges at the Strait of Gibraltar and AMOC during the Late Pliocene and the Late Quaternary (Rogerson et al., 2012; García-Gallardo et al., 2018). As previously inferred from other marine records in the Gulf of Cadiz, the intensification of the MOW could have played a role in the intensification or reinvigoration of AMOC, during the last deglaciation (Rogerson et al., 2006), at the end of Heinrich Stadials (Voelker et al., 2006) or during MIS5e (Bahr et al., 2015).

The activation of the MOW_U (1) is observed just before the massive terminal ice rafting event in the North Atlantic occurring during deglaciation V (Oppo et al., 1998) and (2) is contemporaneous with a decrease of benthic $\delta^{13}\text{C}$ values at North Atlantic sites (ODP Site 980 and IODP Site U1313), which is interpreted as a diminution of North Atlantic Deep Water production (Fig. 13). Despite variations of intensity, the general behaviour of the MOW was probably similar during deglaciation V and the last deglaciation. Consequently, as proposed by many authors for the deglaciation I (e.g., Rogerson et al., 2006; Voelker et al., 2006), MOW may have played an important role in maintaining the AMOC, and particularly its upper branch (Sarthein et al., 2018), during the period of weak NADW formation which characterized the deglaciation V. However, the stimulation of the upper AMOC during the Heinrich Stadials by increasing salinity at intermediate depth and the subsequent transport of moisture to the high latitudes (Bahr et al., 2015), had the potential to strongly impact global climate. This supply of moisture may have contributed to the growth of especially large northern hemisphere ice sheets which may have, in turn, contributed to their destabilization. Thus participating to the “excess” of ice on ice sheets at the end of MIS 12, which was the major factor of Heinrich Stadial of deglaciation V (Vázquez Riveiros et al., 2013; Bahr et al., 2018; Catunda et al., 2021).

MIS 11c is, in our study area, characterized by a weak MOW_U

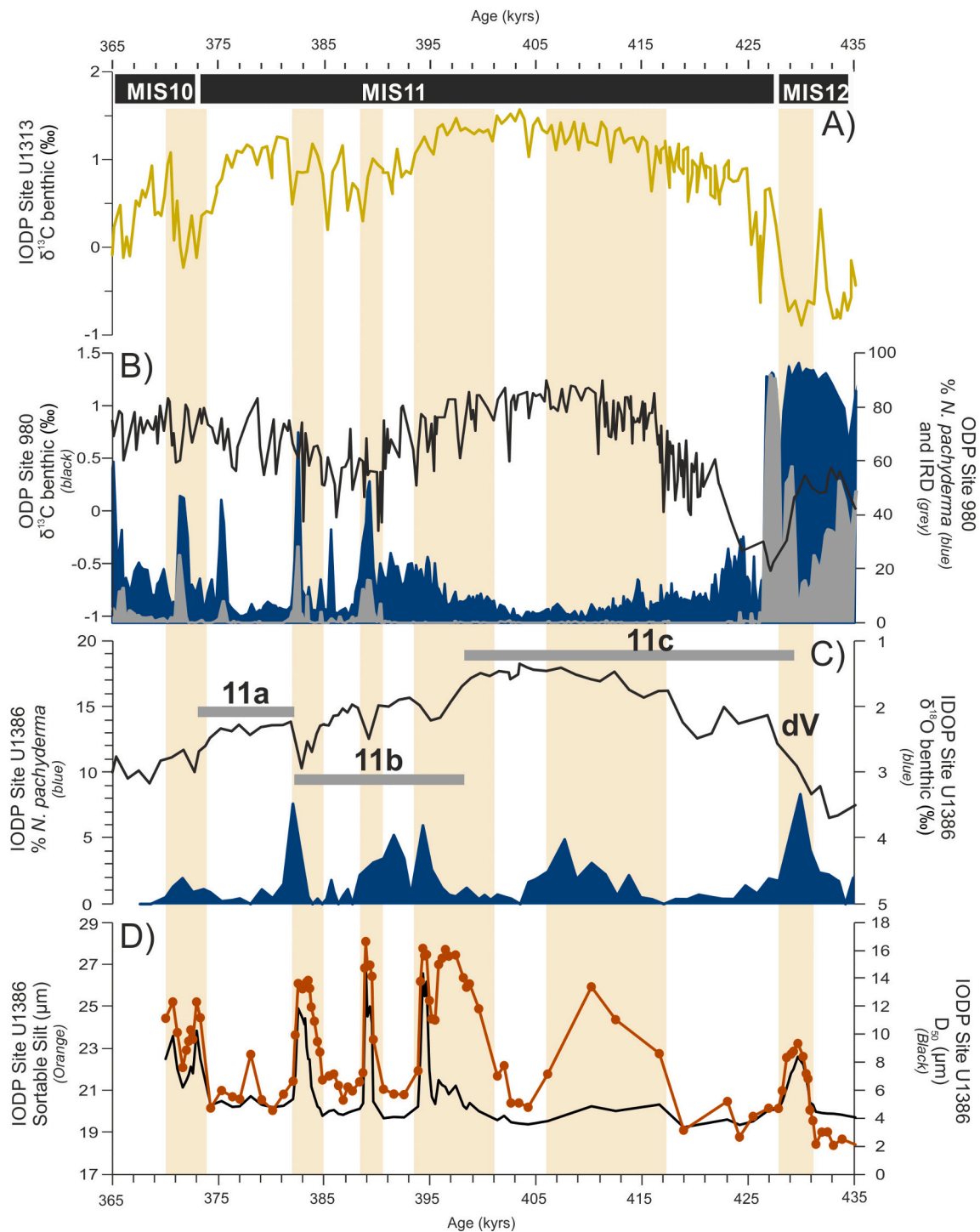


Fig. 13. Mediterranean Upper Water variability and North Atlantic paleoceanography. A) epibenthic $\delta^{13}\text{C}$ record from IODP Site U1313, North Atlantic. B) weight % of IRD (grey), relative abundances of subpolar planktic foraminiferal species (blue [Oppo et al., 1998](#)) and benthic $\delta^{13}\text{C}$ record at ODP Site 980, North Atlantic ([McManus et al., 1999](#)). C) benthic foraminiferal $\delta^{18}\text{O}$ values ([Kaboth et al., 2017](#)) and relative abundances of subpolar planktic foraminifera at IODP Site U1386, Gulf of Cadiz. C: sortable silt (orange symbols) and mean grain size (black) at IODP Site U1386, Gulf of Cadiz. MIS: Marine Isotope Stage. Yellow rectangles: deglaciation V or transition between MIS 12 and MIS 11. (For interpretation of the references to colour in this figure legend, the reader is referred to the web version of this article.)

activity. The slight coarsening of sortable silt associated with the D_{50} which remains stable, only reflects a very low increase of the bottom current velocity ([Fig. 13](#)). Simultaneously, the increase of benthic $\delta^{13}\text{C}$ values at North Atlantic records, indicates a strong NADW production during the MIS 11c ([McManus et al., 1999](#); [Voelker et al., 2010](#)). By contrast, at the transition between the MIS 11c and MIS 11b, there is a

significant strengthening of MOW_U reflected by the simultaneous increase of sortable silt and D_{50} and a progressive reduction of NADW formation ([Fig. 13](#)). These results support previous suggestions of a negative feedback between deep AMOC and MOW_U during MIS 11. This increase of MOW_U activity at the boundary between MIS 11c and MIS 11b ([Fig. 13](#)) may have also strengthened the upper AMOC but the

diminished size and stability of the ice sheet during MIS 11c (McManus et al., 1999) may explain the lack of related IRD in the North Atlantic (Oppo et al., 1998). However, we observe a concomitant increase in both, the abundance of *N. pachyderma* at ODP Site 980, indicative of a drop of SST in North Atlantic, and the flow of the MOW_U (Fig. 13). The moisture supplied by the MOW to high latitude at the end of interglacial MIS 11c may have favoured the growth of ice-sheet, and thus played a role in the transition to the substage MIS 11b.

The behaviour of the MOW_U is similar between the beginning of MIS 11c and the Holocene. During the early part of each interglacial, reduced MOW_U is observed, associated with a sapropel formation in the Eastern Mediterranean Sea. Conversely, the end of each period is characterized by pulses of the MOW_U, but with a considerable difference of bottom current velocity between both interglacials. Consequently, although our results support that North Atlantic overall circulation is similar during MIS 11c and the Holocene (McManus et al., 1999; Rodrigues et al., 2011), it should not be neglected that MOW_U, current intensities might have differed. Interestingly, assuming that the end of the current interglacial would occur in the near future (1.5 kyrs) with CO₂ concentrations lower than 240 ppmv (Tzedakis et al., 2012a), MOW pulses of MIS 11 and Holocene would occur few thousand years (3–6 kyrs) before the onset of the glaciation.

During MIS 11b and at the end of MIS 11a, MOW_U strengthening preceded cold events (stadials) in the North Atlantic Ocean as reflected by IRD discharges at ODP Site 980 (Oppo et al., 1998) (Fig. 13). As proposed by Bahr et al. (2015) for MIS 5e, pulses of MOW can invigorate the upper AMOC by increasing the salinity of North Atlantic Ocean water masses at intermediate depth. Such a stimulated upper branch of the overturning circulation contributed to heat and moisture transport towards the high latitudes during this time, thus sustaining initial ice-sheet growth (McManus et al., 1999). The recorded high abundances of *N. pachyderma* at ODP Site 980, which correspond to slight increases of the percentages of the polar planktic species at IODP sites U1386 and U1387 during MIS 11a, indicate that the slight increases of calving or/and size of ice sheets caused a general cooling in the North Atlantic (Fig. 13). SST drops during the MIS 11 were also recorded in the mid-latitudes of the North Atlantic Ocean (U1313) and to the southwest of the Iberian margin (Voelker et al., 2010; Rodrigues et al., 2011). The significant increases of MOW_U activity during MIS 11b and at the end of MIS 11a correspond to slight decreases of benthic $\delta^{13}\text{C}$ values in North Atlantic, which indicate short episodes of decreased NADW production (Fig. 13). These observations further confirm the negative feedback between the deep branch of the AMOC and exchanges of water masses at the Strait of Gibraltar during the MIS 11. These results, as those of García-Gallardo et al. (2018) for the late Pliocene, support the existence of a “negative feedback” between Mediterranean and North Atlantic deep circulation (Rogerson et al., 2010).

7. Conclusions

Our records from IODP sites U1386 and U1387 show that the composition of contourite sequences in the Faro drift, Gulf of Cadíz, is constrained by a balance between MOW_U velocity and sediment supplies. Using sedimentary facies as an indicator of MOW strength, our data extend the model of MOW_U circulation, previously established for the last 140 kyrs, to the MIS 12–11 periods, showing an active MOW_U during warm intervals and deglaciations.

Our grain size and compositional data obtained at IODP sites U1386 and U1387 show clear evidence that, being more influenced by river plumes during periods of lower sea level, contourite sequences have a more terrigenous composition during deglaciations than during interglacials. During deglaciations, in addition to the increase of the bottom current velocity, this input of terrigenous particles may have played an important role on contourite sequences. Our detailed study of MIS 11 contourite sequences revealed compositional and grain size peculiarities, which are unique to Faro drift contourite beds in the Gulf of Cadíz.

Contrary to the general pattern displayed by contourite beds in this area, grain size maxima are not associated with peaks in carbonate content but with higher contributions of terrigenous particles. Rapid changes of environmental conditions in the Gulf of Cadíz leading to sudden increases of river discharges and drastic reductions of foraminiferal populations in the surface waters are thought to explain these intra MIS 11 variabilities in contourite sequences.

Our unprecedented, high resolution record of MOW_U intensity during MIS 12–11 indicates that strengthened circulation of this water mass during deglaciation V and MIS 11 may have had a significant impact on upper AMOC revigorations and associated heat and moisture transport towards the high latitudes.

Declaration of Competing Interest

None.

Acknowledgements

P. Moal-Darrigade is supported by a doctoral scholarship of the French ministry of research. The authors thank the crew and the scientific teams of the IODP Expedition 339 on the *Joides Resolution*. We acknowledge the help provided by the Bremen Core Repository staff during the sampling periods. We also wish to thank J. Niard, E. Brung, A. Chabrierie and L. Devaux for their assistance during sample preparation. Finally, the authors thank the French programmes INSU LEFE (IMAGO) for financial support and INSU Artémis for most of the radiocarbon dating of this study. We also thank Antje Voelker, for his constructive review, which help us to improve the final version of the manuscript.

Appendix A. Supplementary data

Supplementary data to this article can be found online at <https://doi.org/10.1016/j.gloplacha.2021.103721>.

References

- de Abreu, L., Abrantes, F.F., Shackleton, N.J., Tzedakis, P.C., McManus, J.F., Oppo, D.W., Hall, M.A., 2005. Ocean climate variability in the eastern North Atlantic during interglacial marine isotope stage 11: a partial analogue to the Holocene? *Paleoceanography* 20. <https://doi.org/10.1029/2004PA001091>.
- Alonso, B., Ercilla, G., Casas, D., Stow, D.A.V., Rodríguez-Tovar, F.J., Dorador, J., Hernández-Molina, F.-J., 2016. Contourite vs gravity-flow deposits of the Pleistocene Faro Drift (Gulf of Cadiz): sedimentological and mineralogical approaches. *Mar. Geol.* 377, 77–94. <https://doi.org/10.1016/j.margeo.2015.12.016>.
- Ambar, I., 1983. A shallow core of Mediterranean water off western Portugal. *Deep Sea Research Part A. Oceanographic Research Papers* 30, 677–680.
- Ambar, I., Howe, M., 1979. Observations of the Mediterranean outflow—I mixing in the Mediterranean outflow. *Deep Sea Research Part A. Oceanographic Research Papers* 26, 535–554.
- Ambar, I., Serra, N., Brogueira, M.J., Cabeçadas, G., Abrantes, F., Freitas, P., Gonçalves, C., Gonzalez, N., 2002. Physical, chemical and sedimentological aspects of the Mediterranean outflow off Iberia. *Deep-Sea Res. II Top. Stud. Oceanogr.* 49, 4163–4177. [https://doi.org/10.1016/S0967-0645\(02\)00148-0](https://doi.org/10.1016/S0967-0645(02)00148-0).
- Bahr, A., Jiménez-Espejo, F.J., Kolasinac, N., Grunert, P., Hernández-Molina, F.J., Röhl, U., Voelker, A.H.L., Escutia, C., Stow, D.A.V., Hodell, D., Alvarez-Zarikian, C. A., 2014. Deciphering bottom current velocity and paleoclimate signals from contourite deposits in the Gulf of Cadíz during the last 140 kyr: an inorganic geochemical approach. *Geochem. Geophys. Geosyst.* 15, 3145–3160. <https://doi.org/10.1002/2014GC005356>.
- Bahr, A., Kaboth, S., Jiménez-Espejo, F.J., Sierro, F.J., Voelker, A.H.L., Lourens, L., Röhl, U., Reichert, G.J., Escutia, C., Hernández-Molina, F.J., Pross, J., Friedrich, O., 2015. Persistent monsoonal forcing of Mediterranean Outflow Water dynamics during the late Pleistocene. *Geology* 43, 951–954. <https://doi.org/10.1130/G37013.1>.
- Bahr, A., Kaboth, S., Hodell, D., Zeeden, C., Fiebig, J., Friedrich, O., 2018. Oceanic heat pulses fueling moisture transport towards continental Europe across the mid-Pleistocene transition. *Quat. Sci. Rev.* 179, 48–58. <https://doi.org/10.1016/j.quascirev.2017.11.009>.
- Baringer, M.O., Price, J.F., 1999. A review of the physical oceanography of the Mediterranean outflow. *Mar. Geol.* 155, 63–82. [https://doi.org/10.1016/S0025-3227\(98\)00141-8](https://doi.org/10.1016/S0025-3227(98)00141-8).
- Bassetti, M.-A., Carbonel, P., Sierro, F.J., Perez-Folgado, M., Jouët, G., Berné, S., 2010. Response of ostracods to abrupt climate changes in the Western Mediterranean (Gulf

- of Lions) during the last 30kyr. *Mar. Micropaleontol.* 77 (1–2), 1–14. <https://doi.org/10.1016/j.marmicro.2010.06.004>.
- Be, A.W.H., 1960. Ecology of Recent planktonic foraminifera—Part 2, Bathymetric and seasonal distributions in the Sargasso Sea off Bermuda. *Micropaleontology* 6, 373–392.
- Bigg, G.R., Wadley, M.R., 2001. Millennial-scale variability in the oceans: an ocean modelling view. *J. Quat. Sci.* 16, 309–319. <https://doi.org/10.1002/jqs.599>.
- Billups, K., Hudson, C., Kunz, H., Rew, I., 2016. Exploring Globorotalia truncatulinoides coiling ratios as a proxy for subtropical gyre dynamics in the northwestern Atlantic Ocean during late Pleistocene Ice Ages. *Paleoceanography* 31, 553–563. <https://doi.org/10.1002/2016PA002927>.
- Billups, K., Vizcaíno, M., Chiarello, J., Kaiser, E.A., 2020. Reconstructing Western Boundary Current Stability in the North Atlantic Ocean for the past 700 Kyr from Globorotalia truncatulinoides Coiling Ratios. *Paleoceanography and Paleoclimatology* 35. <https://doi.org/10.1029/2020PA003958> e2020PA003958.
- Borenäs, K., Wåhlin, A., Ambar, I., Serra, N., 2002. The Mediterranean outflow splitting—a comparison between theoretical models and CANIGO data. *Deep-Sea Res. II Top. Stud. Oceanogr.* 49, 4195–4205.
- Bowen, D.Q., 2010. Sea level ~400 000 years ago (MIS 11): analogue for present and future sea-level? *Clim. Past* 6, 19–29. <https://doi.org/10.5194/cp-6-19-2010>.
- Brackenridge, R.E., Hernández-Molina, F.J., Stow, D.A.V., Llave, E., 2013. A Pliocene mixed contourite–turbidite system offshore the Algarve margin, Gulf of Cadiz: Seismic response, margin evolution and reservoir implications. *Mar. Pet. Geol.* 46, 36–50. <https://doi.org/10.1016/j.marpetgeo.2013.05.015>.
- Brackenridge, R.E., Stow, D.A.V., Hernández-Molina, F.J., Jones, C., Mena, A., Alejo, I., Ducassou, E., Llave, E., Ercilla, G., Nombela, M.A., Perez-Arlucea, M., Frances, G., 2018. Textural characteristics and facies of sand-rich contourite depositional systems. *Sedimentology* 65, 2223–2252. <https://doi.org/10.1111/sed.12463>.
- Brunner, C.A., 1986. Deposition of a muddy sediment drift in the southern Straits of Florida during the late Quaternary. *Mar. Geol.* 69, 235–249. [https://doi.org/10.1016/0025-3227\(86\)90041-1](https://doi.org/10.1016/0025-3227(86)90041-1).
- Bryden, H.L., Stommel, H.M., 1984. Limiting processes. *Oceanol. Acta* 7, 289–296.
- Bryden, H.L., Candela, J., Kinder, T.H., 1994. Exchange through the Strait of Gibraltar. *Prog. Oceanogr.* 33, 201–248. [https://doi.org/10.1016/0079-6611\(94\)90028-0](https://doi.org/10.1016/0079-6611(94)90028-0).
- Cacho, I., Shackleton, N., Elderfield, H., Sierro, F.J., Grimalt, J.O., 2006. Glacial rapid variability in deep-water temperature and δ18O from the Western Mediterranean Sea. *Quat. Sci. Rev.* 25 (23–24), 3294–3311. <https://doi.org/10.1016/j.quascirev.2006.10.004>.
- Cacho, I., Grimalt, J.O., Sierro, F.J., Shackleton, N., Canals, M., 2000. Evidence for enhanced Mediterranean thermohaline circulation during rapid climatic coolings. *Earth Planet. Sci. Lett.* 3–4, 417–429. [https://doi.org/10.1016/S0012-821X\(00\)00296-X](https://doi.org/10.1016/S0012-821X(00)00296-X).
- Carracedo, L.L., Pardo, P.C., Flecha, S., Pérez, F.F., 2016. On the Mediterranean Water Composition. *J. Phys. Oceanogr.* 46, 1339–1358. <https://doi.org/10.1175/JPO-D-15-0095.1>.
- Catunda, M.C.A., Bahr, A., Kaboth-Bahr, S., Zhang, X., Foukal, N.P., Friedrich, O., 2021. Subsurface heat channel drove sea surface warming in the high-latitude North Atlantic during the Mid-Pleistocene transition. *Geophys. Res. Lett.* 48 <https://doi.org/10.1029/2020GL091899> e2020GL091899.
- Cavaleiro, C., Voelker, A.H.L., Stoll, H., Baumann, K.-H., Kucera, M., 2020. Coccolithophore productivity at the western Iberian margin during the Middle Pleistocene (310–455 ka) – evidence from coccolith Sr/ca data. *Clim. Past* 16, 2017–2037. <https://doi.org/10.5194/cp-16-2017-2020>.
- Demirov, E.K., Pinardi, N., 2007. On the relationship between the water mass pathways and eddy variability in the Western Mediterranean Sea. *J. Geophys. Res.* 112 <https://doi.org/10.1029/2005JC003174>.
- Droxler, A.W., Farrell, J.W., 2000. Marine Isotope Stage 11 (MIS 11): new insights for a warm future. *Glob. Planet. Chang.* 24, 1–5. [https://doi.org/10.1016/S0921-8181\(99\)00065-X](https://doi.org/10.1016/S0921-8181(99)00065-X).
- Ducassou, E., Hassan, R., Gonthier, E., Duprat, J., Hanquiez, V., Mulder, T., 2018. Biostratigraphy of the last 50 kyr in the contourite depositional system of the Gulf of Cádiz. *Mar. Geol.* 395, 285–300. <https://doi.org/10.1016/j.margeo.2017.09.014>.
- Elderfield, H., Ferretti, P., Greaves, M., Crowhurst, S., McCave, I.N., Hodell, D., Piotrowski, A.M., 2012. Evolution of Ocean temperature and ice volume through the Mid-Pleistocene climate transition. *Science* 337, 704–709. <https://doi.org/10.1126/science.1221294>.
- Ericson, D.B., Wollin, G., 1968. Pleistocene climates and chronology in deep-sea sediments. *Science* 162, 1227–1234.
- Expedition 339 Scientists, 2012. *Mediterranean Outflow: Environmental Significance of the Mediterranean Outflow Water and its Global Implications*. IODP Prel. Rept, p. 339.
- Eynaud, F., de Abreu, L., Voelker, A., Schönfeld, J., Salgueiro, E., Turon, J.-L., Penaud, A., Toucanne, S., Naughton, F., Sánchez Goñi, M.F., Malaizé, B., Cacho, I., 2009. Position of the Polar Front along the western Iberian margin during key cold episodes of the last 45 ka. *Geochem. Geophys. Geosyst.* 10 <https://doi.org/10.1029/2009GC002398>.
- Faugères, J.-C., Gonthier, E., Stow, D.A.V., 1984. Contourite drift molded by deep Mediterranean outflow. *Geology* 12, 296–300. [https://doi.org/10.1130/0091-7613\(1984\)12<296:CDMBDM>2.0.CO;2](https://doi.org/10.1130/0091-7613(1984)12<296:CDMBDM>2.0.CO;2).
- Faugères, J.-C., Gonthier, E., Peypouquet, J., Pujol, C., Vergnaud-Grazzini, C., 1986. Distribution et variations des courants de fond sur la rive de Faro (Golfe de Cadix), témoins des modifications des échanges Méditerranée-Atlantique au Quaternaire récent. *Bulletin de la Société Géologique de France* 2, 423–432.
- Frigola, J., Moreno, A., Cacho, I., Canals, M., Sierro, F.J., Flores, J.A., Grimalt, J.O., 2008. Evidence of abrupt changes in Western Mediterranean Deep Water circulation during the last 50kyr: a high-resolution marine record from the Balearic Sea. *Quat. Int.* 181, 88–104. <https://doi.org/10.1016/j.quaint.2007.06.016>.
- García, M., Hernández-Molina, F.J., Llave, E., Stow, D.A.V., León, R., Fernández-Puga, M. C., Diaz del Río, V., Somoza, L., 2009. Contourite erosive features caused by the Mediterranean Outflow Water in the Gulf of Cadiz: Quaternary tectonic and oceanographic implications. *Mar. Geol.* 257, 24–40. <https://doi.org/10.1016/j.margeo.2008.10.009>.
- García-Gallardo, Á., Grunert, P., Piller, W.E., 2018. Variations in Mediterranean–Atlantic exchange across the late Pliocene climate transition. *Clim. Past* 14, 339–350. <https://doi.org/10.5194/cp-14-339-2018>.
- Gonthier, E., Faugères, J.-C., Stow, D., 1984. Contourite facies of the Faro drift, Gulf of Cadiz. *Geol. Soc. Lond., Spec. Publ.* 15, 275–292. <https://doi.org/10.1144/GSL.SP.1984.015.01.18>.
- Hanquiez, V., 2006. *Processus sédimentaires et activité de la Veine d’Eau Méditerranéenne au cours du Quaternaire terminal dans le Golfe de Cadix*. Université de Bordeaux, Pessac.
- Hanquiez, V., Mulder, T., Lecroart, P., Gonthier, E., Marchès, E., Voisset, M., 2007. High resolution seafloor images in the Gulf of Cadiz, Iberian margin. *Mar. Geol.* 246, 42–59. <https://doi.org/10.1016/j.margeo.2007.08.002>.
- Harris, P.T., Brancolini, G., Armand, L., Busetti, M., Beaman, R.J., Giorgetti, G., Presti, M., Trincardi, F., 2001. Continental shelf drift deposit indicates non-steady state Antarctic bottom water production in the Holocene. *Mar. Geol.* 179, 1–8. [https://doi.org/10.1016/S0025-3227\(01\)00183-9](https://doi.org/10.1016/S0025-3227(01)00183-9).
- Heezen, B.C., Hollister, C.D., Ruddiman, W.F., 1966. Shaping of the continental rise by deep geostrophic contour currents. *Science* 152, 502–508.
- Hernández-Molina, F.J., Llave, E., Stow, D.A.V., García, M., Somoza, L., Vázquez, J.T., Lobo, F.J., Maestro, A., Díaz del Río, V., León, R., Medialdea, T., Gardner, J., 2006. The contourite depositional system of the Gulf of Cádiz: a sedimentary model related to the bottom current activity of the Mediterranean outflow water and its interaction with the continental margin. *Deep-Sea Res. II Top. Stud. Oceanogr.* 53, 1420–1463. <https://doi.org/10.1016/j.dsr2.2006.04.016>.
- Hernández-Molina, F.J., Serra, N., Stow, D.A.V., Llave, E., Ercilla, G., Van Rooij, D., 2011. Along-slope oceanographic processes and sedimentary products around the Iberian margin. *Geo-Mar. Lett.* 31, 315–341. <https://doi.org/10.1007/s00367-011-0242-2>.
- Hernández-Molina, F.J., Stow, D., Alvarez-Zarikian, C., Expedition IODP 339 Scientists, 2013. IODP Expedition 339 in the Gulf of Cadiz and off West Iberia: decoding the environmental significance of the Mediterranean outflow water and its global influence. *Sci. Dril.* 16, 1–11. <https://doi.org/10.5194/sd-16-1-2013>.
- Hernández-Molina, F.J., Llave, E., Preu, B., Ercilla, G., Fontan, A., Bruno, M., Serra, N., Gomiz, J.J., Brackenridge, R.E., Sierro, F.J., Stow, D.A.V., García, M., Juan, C., Sandoval, N., Arnaiz, A., 2014. Contourite processes associated with the Mediterranean Outflow Water after its exit from the Strait of Gibraltar: global and conceptual implications. *Geology* 42, 227–230. <https://doi.org/10.1130/G35083.1>.
- Hernández-Molina, F.J., Sierro, F.J., Llave, E., Roque, C., Stow, D.A.V., Williams, T., Lofi, J., Van der Schee, M., Arnáiz, A., Ledesma, S., Rosales, C., Rodríguez-Tovar, F. J., Pardo-Igúzquiza, E., Brackenridge, R.E., 2016. Evolution of the gulf of Cadiz margin and Southwest Portugal contourite depositional system: Tectonic, sedimentary and paleoceanographic implications from IODP expedition 339. *Mar. Geol.* 377, 7–39. <https://doi.org/10.1016/j.margeo.2015.09.013>.
- Hernández-Molina, F.J., Llave, E., Somoza, L., Fernández-Puga, M.C., Maestro, A., León, R., Medialdea, T., Barnolas, A., García, M., del Río, V.D., Rodero, J., Gardner, J., 2003. Looking for clues to paleoceanographic imprints: a diagnosis of the Gulf of Cadiz contourite depositional systems. *Geology* 31, 19–22. [https://doi.org/10.1130/0091-7613\(2003\)031<0019:LFCTPI>2.0.CO;2](https://doi.org/10.1130/0091-7613(2003)031<0019:LFCTPI>2.0.CO;2).
- Hodell, D., Lourens, L., Crowhurst, S., Konijnendijk, T., Tjallingii, R., Jiménez Espejo, F., Skinner, L., Tzedakis, P.C., Abrantes, F., Acton, G.D., Alvarez Zarikian, C.A., Bahr, A., Balestra, B., Llave Barranco, E., Carrara, G., Ducassou, E., Flood, R.D., Flores, J.-A., Furota, S., Grimalt, J., Grunert, P., Hernández-Molina, J., Kim, J.K., Kriesek, L.A., Kuroda, J., Li, B., Lofi, J., Margari, V., Martrat, B., Miller, M.D., Nanayama, F., Nishida, N., Richter, C., Rodrigues, T., Rodríguez-Tovar, F.J., Freixo Roque, A.C., Sánchez Goñi, M.F., Sierro Sánchez, F.J., Singh, A.D., Sloss, C.R., Stow, D.A.V., Takashimizu, Y., Tzanova, A., Voelker, A., Xuan, C., Williams, T., 2015. A Reference Time Scale for Site U1385 (Shackleton site) on the SW Iberian Margin. Affiliation (analytic): University of Cambridge, Department of Earth Sciences, Cambridge Affiliation (monographic): University of Cambridge, Department of Earth Sciences, Cambridge, United Kingdom Corporate Affiliation (monographic): Shackleton Site Project Members Coordinates: N373417 N373417 W0100719 W0100720 illus., incl. table, sketch map Contains 61 references Research Program: IODP Integrated Ocean Drilling Program Document Type: Journal Article Bibliographic Level: Analytic Source Note: Global and Planetary Change, Vol.133, p.49-64. Publisher: Elsevier, Amsterdam, Netherlands. ISSN: 0921-8181 Copyright Information: GeoRef, Copyright 2019 American Geosciences Institute. Reference includes data from CAPCAS, Elsevier Scientific Publishers, Amsterdam, Netherlands GeoRef ID: 2016037553 DOI: <https://doi.org/10.1016/j.gloplacha.2015.07.002.133>, 49.
- Ivanovic, R.F., Valdes, P.J., Flecker, R., Gregoire, L.J., Gutjahr, M., 2013. The parameterisation of Mediterranean–Atlantic water exchange in the Hadley Centre model HadCM3, and its effect on modelled North Atlantic climate. *Ocean Model.* 62, 11–16. <https://doi.org/10.1016/j.ocemod.2012.11.002>.
- Jouzel, J., Masson-Delmotte, V., Cattani, O., Dreyfus, G., Falourd, S., Hoffmann, G., Minster, B., Nouet, J., Barnola, J.M., Chappellaz, J., Fischer, H., Gallet, J.C., Johnsen, S., Leuenberger, M., Loulergue, L., Luethi, D., Oerter, H., Parrenin, F., Raisbeck, G., Raynaud, D., Schilt, A., Schwander, J., Selmo, E., Souchez, R., Spahni, R., Stauffer, B., Steffensen, J.P., Stenni, B., Stocker, T.F., Tison, J.L., Werner, M., Wolff, E.W., 2007. Orbital and Millennial Antarctic climate Variability

- over the past 800,000 years. *Science* 317, 793–796. <https://doi.org/10.1126/science.1141038>.
- Kaboth, S., Bahr, A., Reichart, G.-J., Jacobs, B., Lourens, L.J., 2016. New insights into upper MOW variability over the last 150kyr from IODP 339 Site U1386 in the Gulf of Cadiz. *Mar. Geol.* 377, 136–145. <https://doi.org/10.1016/j.margeo.2015.08.014>.
- Kaboth, S., de Boer, B., Bahr, A., Zeeden, C., Lourens, L.J., 2017. Mediterranean Outflow Water dynamics during the past ~570 kyr: Regional and global implications: Middle to late Pleistocene MOW. *Paleoceanography* 32, 634–647. <https://doi.org/10.1002/2016PA003063>.
- Kaiser, E.A., Caldwell, A., Billups, K., 2019. North Atlantic Upper-Ocean Hydrography during the Mid-Pleistocene transition evidenced by Globorotalia truncatulinoides Coiling Ratios. *Paleoceanography and Paleoclimatology* 34, 658–671. <https://doi.org/10.1029/2018PA003502>.
- Khélifi, N., Sarnthein, M., Frank, M., Andersen, N., Garbe-Schönberg, D., 2014. Late Pliocene variations of the Mediterranean outflow. *Mar. Geol.* 357, 182–194. <https://doi.org/10.1016/j.margeo.2014.07.006>.
- Konijnendijk, T.Y.M., Ziegler, M., Lourens, L.J., 2014. Chronological constraints on Pleistocene sapropel depositions from high-resolution geochemical records of ODP Sites 967 and 968. *Newsl. Stratigr.* 263–282. <https://doi.org/10.1127/0078-0421/2014/0047>.
- Lisiecki, L.E., Raymo, M.E., 2005. A Pliocene-Pleistocene stack of 57 globally distributed benthic $\delta^{18}O$ records: Pliocene-PLEISTOCENE BENTHIC STACK. *Paleoceanography* 20, n/a-n/a. <https://doi.org/10.1029/2004PA001071>.
- Llave, E., Schönfeld, J., Hernández-Molina, F.J., Mulder, T., Somoza, L., Díaz del Río, V., Sánchez-Almazo, I., 2006. High-resolution stratigraphy of the Mediterranean outflow contourite system in the Gulf of Cadiz during the late Pleistocene: the impact of Heinrich events. *Mar. Geol.* 227, 241–262. <https://doi.org/10.1016/j.margeo.2005.11.015>.
- Llave, E., Hernández-Molina, F.J., Somoza, L., Stow, D., Del Río, V.D., 2007. Quaternary evolution of the contourite depositional system in the Gulf of Cadiz. *Geol. Soc. Lond., Spec. Publ.* 276, 49–79.
- Lofi, J., Voelker, A.H.L., Ducassou, E., Hernández-Molina, F.J., Sierro, F.J., Bahr, A., Galvani, A., Lourens, L.J., Pardo-Igúzquiza, E., Pezard, P., Rodríguez-Tovar, F.J., Williams, T., 2016. Quaternary chronostratigraphic framework and sedimentary processes for the Gulf of Cadiz and Portuguese Contourite Depositional Systems derived from Natural Gamma Ray records. *Mar. Geol.* 377, 40–57. <https://doi.org/10.1016/j.margeo.2015.12.005>.
- Loutre, M.F., Berger, A., 2000. Future climatic changes: are we entering an exceptionally long interglacial? *Clim. Chang.* 46, 61–90. <https://doi.org/10.1023/A:1005559827189>.
- Loutre, M.F., Berger, A., 2003. Marine isotope stage 11 as an analogue for the present interglacial. *Glob. Planet. Chang.* 36, 209–217. [https://doi.org/10.1016/S0921-8181\(02\)00186-8](https://doi.org/10.1016/S0921-8181(02)00186-8).
- Madelain, F., 1970. Influence de la topographie du fond sur l'écoulement méditerranéen entre le Déroit de Gibraltar et le Cap Saint-Vincent. *Cahiers Océanogr.* 22, 43–61.
- Marchès, E., Mulder, T., Cremer, M., Bonnel, C., Hanquiez, V., Gonthier, E., Lecroart, P., 2007. Contourite drift construction influenced by capture of Mediterranean Outflow Water deep-sea current by the Portimão submarine canyon (Gulf of Cadiz, South Portugal). *Mar. Geol.* 242, 247–260. <https://doi.org/10.1016/j.margeo.2007.03.013>.
- McCave, I.N., Hall, I.R., 2006. Size sorting in marine muds: processes, pitfalls, and prospects for paleoflow-speed proxies: SIZE SORTING IN MARINE MUDDS. *Geochem. Geophys. Geosyst.* 7 <https://doi.org/10.1029/2006GC001284> n/a-n/a.
- McCave, I.N., Manighetti, B., Robinson, S.G., 1995. Sortable silt and fine sediment size/composition slicing: parameters for palaeocurrent speed and palaeoceanography. *Paleoceanography* 10, 18. <https://doi.org/10.1029/94PA03039>.
- Mcmantas, J., Oppo, D., Cullen, J., Healey, S., 2003. Marine Isotope Stage 11 (Mis 11): Analog for Holocene and Future Climate?. In: *Earth's Climate and Orbital Eccentricity: The Marine Isotope Stage 11 Question*. American Geophysical Union (AGU), pp. 69–85. <https://doi.org/10.1029/137GM06>.
- McManus, J.F., Oppo, D.W., Cullen, J.L., 1999. A 0.5-Million-Year Record of Millennial-Scale climate Variability in the North Atlantic. *Science* 283, 971–975. <https://doi.org/10.1126/science.283.5404.971>.
- Mestdagh, T., Lobo, F.J., Llave, E., Hernández-Molina, F.J., Van Rooij, D., 2019. Review of the late Quaternary stratigraphy of the northern Gulf of Cadiz continental margin: New insights into controlling factors and global implications. *Earth Sci. Rev.* 198, 102944 <https://doi.org/10.1016/j.earscirev.2019.102944>.
- Millot, C., 2009. Another description of the Mediterranean Sea outflow. *Prog. Oceanogr.* 82, 101–124. <https://doi.org/10.1016/j.pocean.2009.04.016>.
- Millot, C., 2014. Heterogeneities of in-and out-flows in the Mediterranean Sea. *Prog. Oceanogr.* 120, 254–278. <https://doi.org/10.1016/j.pocean.2013.09.007>.
- Millot, C., Candelá, J., Fuda, J.-L., Tber, Y., 2006. Large warming and salinification of the Mediterranean outflow due to changes in its composition. *Deep-Sea Res. I Oceanogr. Res. Pap.* 53, 656–666.
- Mulder, T., Lecroart, P., Hanquiez, V., Marchès, E., Gonthier, E., Guedes, J.-C., Thiébot, E., Jaaidi, B., Kenyon, N., Voisset, M., Perez, C., Sayago, M., Fuchey, Y., Bujan, S., 2006. The western part of the Gulf of Cadiz: contour currents and turbidity currents interactions. *Geo-Mar. Lett.* 26, 31–41. <https://doi.org/10.1007/s00367-005-0013-z>.
- Mulder, T., Hassan, R., Ducassou, E., Zaragosi, S., Gonthier, E., Hanquiez, V., Marchès, E., Toucanne, S., 2013. Contourites in the Gulf of Cadiz: a cautionary note on potentially ambiguous indicators of bottom current velocity. *Geo-Mar. Lett.* 33, 357–367. <https://doi.org/10.1007/s00367-013-0332-4>.
- Mulder, T., Lecroart, T.P., Voisset, M., Schönfeld, J., Le Drezén, E., Gonthier, E., Hanquiez, V., Zahn, R., Faugères, J.-C., Hernandez-Molina, F.J., Llave-Barranco, E., Gervais, A., 2002. Past deep-ocean circulation and the paleoclimate record-Gulf of Cadiz. *Eos, Transactions American Geophysical Union* 43, 481–488. <https://doi.org/10.1029/2002EO000337>.
- Naranjo, C., Sarmartino, S., García-Lafuente, J., Bellanco, M.J., Taupier-Letage, I., 2015. Mediterranean waters along and across the Strait of Gibraltar, characterization and zonal modification. *Deep-Sea Res. I Oceanogr. Res. Pap.* 105, 41–52. <https://doi.org/10.1016/j.dsr.2015.08.003>.
- Nelson, C.H., Maldonado, A., 1999. The Cadiz margin study off Spain: an introduction. *Mar. Geol.* 155, 3–8. [https://doi.org/10.1016/S0025-3227\(98\)00138-8](https://doi.org/10.1016/S0025-3227(98)00138-8).
- Oliveira, D., Desprat, S., Rodrigues, T., Naughton, F., Hodell, D., Trigo, R., Rufino, M., Lopes, C., Abrantes, F., Goni, M.F.S., 2016. The complexity of millennial-scale variability in southwestern Europe during MIS 11. *Quat. Res.* 86, 373–387. <https://doi.org/10.1016/j.yqres.2016.09.002>.
- Oppo, D.W., McManus, J.L., Cullen, J.L., 1998. Abrupt climate events 500,000 to 340,000 years ago: evidence from Subpolar North Atlantic sediments. *Science* 279, 1335–1338. <https://doi.org/10.1126/science.279.5355.1335>.
- Palumbo, E., Voelker, A.H.L., Flores, J.A., Amore, O.F., 2019. Surface-ocean dynamics during eccentricity minima: a comparison between interglacial Marine Isotope Stage (MIS) 1 and MIS 11 on the Iberian margin. *Glob. Planet. Chang.* 172, 242–255. <https://doi.org/10.1016/j.gloplacha.2018.10.011>.
- Pepple, I.B., 2020. Chapter 6: Sediments and textures. *Morphostructure and tectono-sedimentary control of a mixed contourite-turbidite system in a transpressive margin: Gulf of Cadiz, SW Iberia*. Heriot-Watt University, Edinburgh, pp. 328–432.
- Petit, J.R., Jouzel, J., Raynaud, D., Barkov, N.I., Barnola, J.-M., Basile, I., Bender, M., Chappellaz, J., Davis, M., Delaygue, G., Delmotte, M., Kotlyakov, V.M., Legrand, M., Lipenkov, V.Y., Lorius, C., Pépin, R., Ritz, C., Saltzman, E., Stievenard, M., 1999. Climate and atmospheric history of the past 420,000 years from the Vostok ice core, Antarctica. *Nature* 399, 429–436. <https://doi.org/10.1038/20859>.
- Rabineau, M., Berné, S., Olivet, J.-L., Aslanian, D., Guillocheau, F., Joseph, P., 2006. Paleo Sea levels reconsidered from direct observation of paleoshoreline position during Glacial Maxima (for the last 500,000 yr). *Earth Planet. Sci. Lett.* 252, 119–137. <https://doi.org/10.1016/j.epsl.2006.09.033>.
- Rahmstorf, S., 1998. Influence of mediterranean outflow on climate. *Eos Trans. AGU* 79, 281–282. <https://doi.org/10.1029/98EO00208>.
- Railsback, L.B., Gibbard, P.L., Head, M.J., Voarintsoa, N.R.G., Toucanne, S., 2015. An optimized scheme of lettered marine isotope substages for the last 1.0 million years, and the climatostratigraphic nature of isotope stages and substages. *Quat. Sci. Rev.* 111, 94–106. <https://doi.org/10.1016/j.quascirev.2015.01.012>.
- Raynaud, D., Barnola, J.-M., Souchez, R., Lorrain, R., Petit, J.-R., Duval, P., Lipenkov, V. Y., 2005. The record for marine isotopic stage 11. *Nature* 436, 39–40. <https://doi.org/10.1038/43639b>.
- Rebesco, M., Camerlenghi, A., Loon, A.J.V., 2008. Contourite Research: a field in full development. *Developments in Sedimentology* 60, 0–8.
- Rebesco, M., Hernández-Molina, F.J., Van Rooij, D., Wählin, A., 2014. Contourites and associated sediments controlled by deep-water circulation processes: State-of-the-art and future considerations. *Mar. Geol.* 352, 111–154. <https://doi.org/10.1016/j.margeo.2014.03.011>.
- Reid, J.L., 1979. On the contribution of the Mediterranean Sea outflow to the Norwegian-Greenland Sea. *Deep Sea Research Part A. Oceanographic Research Papers* 26, 1199–1223. [https://doi.org/10.1016/0198-0149\(79\)90064-5](https://doi.org/10.1016/0198-0149(79)90064-5).
- Reimer, P.J., Baillie, M.G.L., Bard, E., Bayliss, A., Beck, J.W., Blackwell, P.G., Ramsey, C. B., Buck, C.E., Burr, G.S., Edwards, R.L., Friedrich, M., Grootes, P.M., Guilderson, T. P., Hajdas, I., Heaton, T.J., Hogg, A.G., Hughen, K.A., Kaiser, K.F., Kromer, B., McCormac, F.G., Manning, S.W., Reimer, R.W., Richards, D.A., Southon, J.R., Talamo, S., Turney, C.S.M., 2009. IntCal09 and Marine09 radiocarbon age calibration curves, 0–50,000 years CAL BP. *Radiocarbon* 51, 1111–1150.
- Robinson, S.G., McCave, I.N., 1994. Orbital forcing of bottom-current enhanced sedimentation on Feni Drift, NE Atlantic, during the mid-Pleistocene. *Paleoceanography* 9, 943–972. <https://doi.org/10.1029/94PA01439>.
- Rodrigues, T., Grimalt, J.O., Abrantes, F.G., Flores, J.A., Lebreiro, S.M., 2009. Holocene interdependencies of changes in sea surface temperature, productivity, and fluvial inputs in the Iberian continental shelf (Tagus mud patch). *Geochem. Geophys. Geosyst.* 10 <https://doi.org/10.1029/2008GC002367> n/a-n/a.
- Rodrigues, T., Voelker, A.H.L., Grimalt, J.O., Abrantes, F., Naughton, F., 2011. Iberian margin sea surface temperature during MIS 15 to 9 (580–300 ka): Glacial suborbital variability versus interglacial stability. *Paleoceanography* 26, PA1204. <https://doi.org/10.1029/2010PA001927>.
- Rogerson, M., Rohling, E.J., Weaver, P.P.E., Murray, J.W., 2005. Glacial to interglacial changes in the settling depth of the Mediterranean Outflow plume. *Paleoceanography* 20. <https://doi.org/10.1029/2004PA001106>.
- Rogerson, M., Rohling, E.J., Weaver, P.P.E., 2006. Promotion of meridional overturning by Mediterranean-derived salt during the last deglaciation. *Paleoceanography* 21. <https://doi.org/10.1029/2006PA001306>.
- Rogerson, M., Colmenero-Hidalgo, E., Levine, R.C., Rohling, E.J., Voelker, A.H.L., Bigg, G.R., Schönfeld, J., Cacho, I., Sierro, F.J., Löwemark, L., Reguera, M.I., de Abreu, L., Garrick, K., 2010. Enhanced Mediterranean-Atlantic exchange during Atlantic freshening phases. *Geochem. Geophys. Geosyst.* 11 <https://doi.org/10.1029/2009GC002931> n/a-n/a.
- Rogerson, M., Rohling, E.J., Bigg, G.R., Ramirez, J., 2012. Paleocirculation of the Atlantic-Mediterranean exchange: overview and first quantitative assessment of climatic forcing. *Rev. Geophys.* 50 <https://doi.org/10.1029/2011RG000376>.
- Rohling, E.J., Braun, K., Grant, K., Kucera, M., Roberts, A.P., Siddall, M., Trommer, G., 2010. Comparison between Holocene and Marine Isotope Stage-11 sea-level histories. *Earth Planet. Sci. Lett.* 291, 97–105. <https://doi.org/10.1016/j.epsl.2009.12.054>.

- Rohling, E.J., Hayes, A., De Rijk, S., Kroon, D., Zachariasse, W.J., Eisma, D., 1998. Abrupt cold spells in the northwest Mediterranean. *Paleoceanography* 13 (4), 316–322. <https://doi.org/10.1029/98PA00671>.
- Sanchez Goñi, M.F., Harrison, S.P., 2010. Millennial-scale climate variability and vegetation changes during the last Glacial: concepts and terminology. *Quat. Sci. Rev.* 29, 2823–2827. <https://doi.org/10.1016/j.quascirev.2009.11.014>.
- Sánchez Goñi, M.F., Llave, E., Oliveira, D., Naughton, F., Desprat, S., Ducassou, E., Hodell, D.A., Hernández-Molina, F.J., 2016. Climate changes in south western Iberia and Mediterranean Outflow variations during two contrasting cycles of the last 1Myrs: MIS 31–MIS 30 and MIS 12–MIS 11. *Glob. Planet. Chang.* 136, 18–29. <https://doi.org/10.1016/j.gloplacha.2015.11.006>.
- Sarnthein, M., Grunert, P., Khélifi, N., Frank, M., Nürnberg, D., 2018. Interhemispheric teleconnections: late Pliocene change in Mediterranean outflow water linked to changes in Indonesian Through-Flow and Atlantic Meridional Overturning Circulation, a review and update. *Int J Earth Sci (Geol Rundsch)* 107, 505–515. <https://doi.org/10.1007/s00531-017-1505-6>.
- Schiebel, R., Hemleben, C., 2017. Classification and Taxonomy of Extant Planktic Foraminifers. In: Schiebel, R., Hemleben, C. (Eds.), *Planktic Foraminifers in the Modern Ocean*. Springer, Berlin, Heidelberg, pp. 11–110. https://doi.org/10.1007/978-3-662-50297-6_2.
- Schönfeld, J., Zahn, R., 2000. Late Glacial to Holocene history of the Mediterranean Outflow. Evidence from benthic foraminiferal assemblages and stable isotopes at the Portuguese margin. *Paleoceanogr. Palaeoclimatol. Palaeoecol.* 159, 85–111. [https://doi.org/10.1016/S0031-0182\(00\)00035-3](https://doi.org/10.1016/S0031-0182(00)00035-3).
- Schroeder, K., Chiggiato, J., Josey, S.A., Borghini, M., Aracri, S., Sparnocchia, S., 2017. Rapid response to climate change in a marginal sea. *Sci. Rep.* 7, 1–7.
- Serra, N., Ambar, I., Boutou, D., 2010. Surface expression of Mediterranean Water dipoles and their contribution to the shelf/slope – open ocean exchange. *Ocean Sci.* 19.
- Siegenthaler, U., Stocker, T.F., Monnin, E., Lüthi, D., Schwander, J., Stauffer, B., Raynaud, D., Barnola, J.-M., Fischer, H., Masson-Delmotte, V., Jouzel, J., 2005. Stable carbon cycle–climate relationship during the Late Pleistocene. *Science* 310, 1313–1317. <https://doi.org/10.1126/science.1120130>.
- Sierro, F.J., Flores, J.A., Baraza, J., 1999. Late glacial to recent paleoenvironmental changes in the Gulf of Cadiz and formation of sandy contourite layers. *Mar. Geol.* 155, 157–172. [https://doi.org/10.1016/S0025-3227\(98\)00145-5](https://doi.org/10.1016/S0025-3227(98)00145-5).
- Sierro, F.J., Hodell, D.A., Andersen, N., Azibeiro, L.A., Jimenez-Espejo, F.J., Bahr, A., Flores, J.A., Ausin, B., Rogerson, M., Lozano-Luz, R., others, 2020. Mediterranean overflow over the last 250 kyr: freshwater forcing from the tropics to the ice sheets. *Paleoceanography and Paleoclimatology* 35. <https://doi.org/10.1029/2020PA003931> e2020PA003931.
- Sierro, F.J., Hodell, D.A., Curtis, J.H., Flores, J.A., Reguera, I., Colmenero-Hidalgo, E., Bárcena, M.A., Grimalt, J.O., Cacho, I., Frigola, J., Canals, M., 2005. Impact of iceberg melting on Mediterranean thermohaline circulation during Heinrich events. *Paleoceanography* 20 (2). <https://doi.org/10.1029/2004PA001051>.
- Spahni, R., Chappellaz, J., Stocker, T.F., Loulergue, L., Hausammann, G., Kawamura, K., Flückiger, J., Schwander, J., Raynaud, D., Masson-Delmotte, V., Jouzel, J., 2005. Atmospheric methane and nitrous oxide of the late Pleistocene from Antarctic Ice Cores. *Science* 310, 1317–1321. <https://doi.org/10.1126/science.1120132>.
- Spezzaferri, S., Kucera, M., Pearson, P.N., Wade, B.S., Rappo, S., Poole, C.R., Morard, R., Stalder, C., 2015. Fossil and genetic evidence for the Polyphyletic nature of the Planktonic Foraminifera “Globigerinoides”, and Description of the New Genus *Trilobatus*. *PLoS One* 10, e0128108. <https://doi.org/10.1371/journal.pone.0128108>.
- Stow, D.A., Faugères, J.-C., Howe, J.A., Pudsey, C.J., Viana, A.R., 2002. Bottom currents, contourites and deep-sea sediment drifts: current state-of-the-art. *Geological Society, London, Memoirs* 22, 7–20.
- Stow, D.A., Hernández-Molina, F.J., Llave, E., Sayago-Gil, M., Díaz del Río, V., Branson, A., 2009. Bedform-velocity matrix: the estimation of bottom current velocity from bedform observations. *Geology* 37, 327–330.
- Stow, D.A.V., Faugères, J.-C., Gonthier, E., 1986. Facies distribution and textural variation in Faro Drift contourites: velocity fluctuation and drift growth. *Mar. Geol.* 72, 71–100. [https://doi.org/10.1016/0025-3227\(86\)90100-3](https://doi.org/10.1016/0025-3227(86)90100-3).
- Stow, D.A.V., Hernández-Molina, F.J., Alvarez Zarikian, C.A., Expedition 339 Scientists, 2013. Site U1386. *Proc. IODP*, 339: Tokyo (Integrated Ocean Drilling Program Management International, Inc.). <https://doi.org/10.2204/iodp.proc.339.104.2013>.
- Stow, D.A.V., Hernández-Molina, F.J., Llave, E., Bruno, M., García, M., Díaz del Río, V., Somoza, L., Brackenridge, R.E., 2013. The Cadiz contourite channel: Sandy contourites, bedforms and dynamic current interaction. *Mar. Geol.* 343, 99–114. <https://doi.org/10.1016/j.margeo.2013.06.013>.
- Stumpf, R., Frank, M., Schönfeld, J., Haley, B.A., 2011. Climatically driven changes in sediment supply on the SW Iberian shelf since the last Glacial Maximum. *Earth Planet. Sci. Lett.* 312, 80–90. <https://doi.org/10.1016/j.epsl.2011.10.002>.
- Swingedouw, D., Colin, C., Eynaud, F., Ayache, M., Zaragosi, S., 2019. Impact of freshwater release in the Mediterranean Sea on the North Atlantic climate. *Clim. Dyn.* 53, 3893–3915. <https://doi.org/10.1007/s00382-019-04758-5>.
- Telford, R.J., Heegaard, E., Birks, H.J.B., 2004. The intercept is a poor estimate of a calibrated radiocarbon age. *The Holocene* 14, 296–298. <https://doi.org/10.1191/0959683604hl707fa>.
- Tjallingii, R., Röhl, U., Kölling, M., Bickert, T., 2007. Influence of the water content on X-ray fluorescence core-scanning measurements in soft marine sediments. *Geochem. Geophys. Geosyst.* 8. <https://doi.org/10.1029/2006GC001393>.
- Toucanne, S., Mulder, T., Schönfeld, J., Hanquiez, V., Gonthier, E., Duprat, J., Cremer, M., Zaragosi, S., 2007. Contourites of the Gulf of Cadiz: a high-resolution record of the paleocirculation of the Mediterranean outflow water during the last 50,000 years. *Paleoceanogr. Palaeoclimatol. Palaeoecol.* 246, 354–366. <https://doi.org/10.1016/j.palaeo.2006.10.007>.
- Toucanne, S., Jouet, G., Ducassou, E., Bassetti, M.-A., Dennielou, B., Angue Minto'o, C. M., Lahmi, M., Touyet, N., Charlier, K., Lericolais, G., Mulder, T., 2012. A 130,000-year record of Levantine intermediate water flow variability in the Corsica Trough, western Mediterranean Sea. *Quat. Sci. Rev.* 33, 55–73. <https://doi.org/10.1016/j.quascirev.2011.11.020>.
- Turon, J.-L., Lézine, A.-M., Denèfle, M., 2003. Land–sea correlations for the last glaciation inferred from a pollen and dinocyst record from the Portuguese margin. *Quat. Res.* 59, 88–96. [https://doi.org/10.1016/S0033-5894\(02\)00018-2](https://doi.org/10.1016/S0033-5894(02)00018-2).
- Tzedakis, P.C., Channell, J.E.T., Hodell, D.A., Kleiven, H.F., Skinner, L.C., 2012a. Determining the natural length of the current interglacial. *Nat. Geosci.* 5, 138–141. <https://doi.org/10.1038/ngeo1358>.
- Tzedakis, P.C., Wolff, E.W., Skinner, L.C., Brovkin, V., Hodell, D.A., McManus, J.F., Raynaud, D., 2012b. Can we predict the duration of an interglacial? *Clim. Past* 8, 1473–1485. <https://doi.org/10.5194/cp-8-1473-2012>.
- Vázquez Riveiros, N., Waelbroeck, C., Skinner, L., Duplessy, J.-C., McManus, J.F., Kandiano, E.S., Bauch, H.A., 2013. The “MIS 11 paradox” and ocean circulation: Role of millennial scale events. *Earth Planet. Sci. Lett.* 371–372, 258–268. <https://doi.org/10.1016/j.epsl.2013.03.036>.
- Voelker, A., Lebreiro, S., Schönfeld, J., Cacho, I., Erlenkeuser, H., Abrantes, F., 2006. Mediterranean outflow strengthening during northern hemisphere coolings: a salt source for the glacial Atlantic? *Earth Planet. Sci. Lett.* 245, 39–55. <https://doi.org/10.1016/j.epsl.2006.03.014>.
- Voelker, A.H.L., de Abreu, L., Schönfeld, J., Erlenkeuser, H., Abrantes, F., 2009. Hydrographic conditions along the western Iberian margin during marine isotope stage 2. *Geochem. Geophys. Geosyst.* 10. <https://doi.org/10.1029/2009GC002605>.
- Voelker, A.H.L., Rodrigues, T., Billups, K., Oppo, D., McManus, J., Stein, R., Hefter, J., Grimalt, J.O., 2010. Variations in mid-latitude North Atlantic surface water properties during the mid-Brunhes (MIS 9–14) and their implications for the thermohaline circulation. *Clim. Past* 6, 531–552. <https://doi.org/10.5194/cp-6-531-2010>.
- Voelker, A.H.L., Salgueiro, E., Rodrigues, T., Jimenez-Espejo, F.J., Bahr, A., Alberto, A., Loureiro, I., Padilha, M., Rebotim, A., Roehl, U., 2015a. Mediterranean Outflow and surface water variability off southern Portugal during the early Pleistocene: a snapshot at Marine Isotope Stages 29 to 34 (1020–1135 ka). *Glob. Planet. Chang.* 133, 223–237. <https://doi.org/10.1016/j.gloplacha.2015.08.015>.
- Voelker, A.H.L., Colman, Albert, Olack, Gerard, Waniek, Joanna J., Hodell, David, 2015b. Oxygen and hydrogen isotope signatures of Northeast Atlantic water masses. *Deep-Sea Research II* 116, 89–106. <https://doi.org/10.1016/j.dsr2.2014.11.006>.
- Waelbroeck, C., Labeyrie, L., Michel, E., Duplessy, J.C., McManus, J.F., Lambeck, K., Balbon, E., Labracherie, M., 2002. Sea-level and deep water temperature changes derived from benthic foraminifera isotopic records. *Quat. Sci. Rev.* 21, 295–305. [https://doi.org/10.1016/S0277-3791\(01\)00101-9](https://doi.org/10.1016/S0277-3791(01)00101-9).
- Wu, W., Danabasoglu, G., Large, W.G., 2007. On the effects of parameterized Mediterranean overflow on North Atlantic Ocean circulation and climate. *Ocean Model.* 19, 31–52. <https://doi.org/10.1016/j.ocemod.2007.06.003>.